Late Pleistocene Sea Levels and

Resulting Changes in Global Land Distributions

BY

Cheng Zong

Submitted to the graduate degree program in Geography and the Graduate Faculty of the University of Kansas in partial fulfillment of the requirements for the degree of Master of Science.

_____

Chair: Jerome E. Dobson

_____

Stephen Egbert

_____

Xingong Li

Date Defended: May 13, 2015

The Thesis Committee for Cheng Zong

certifies that this is the approved version of the following thesis:

Late Pleistocene Sea Levels and

Resulting Changes in Global Land Distributions

_____

Jerome E. Dobson, Chair

Date approved: June 10, 2015

Late Pleistocene Sea Levels and Resulting Changes in Global Land Distributions

Abstract

Over the past 120,000 years global sea level has fluctuated through multiple cycles of rises and falls, ranging from a few meters above current level to 139 meters below. This thesis analyzes the resulting distributions of terrestrial and submerged lands at regular intervals of 1,000 years. Global mean sea level change is derived from 12 *in situ* database interpolated temporally with various fitting models. Some sea levels are based on single *in situ* observations at specific time windows. The fitting models including Fourier series, sum of sine, smoothing spline, and central tendency measurements are used for predicting data curves. Two methods, employed to see if a trend exists throughout the past 120,000 years, are linear regression and TFPW Mann-Kendall trend test. An animation about terrestrial vs. submerged land change is made to show global changes in the extent of aquaterra, defined as the lands that were alternately exposed and inundated as ice sheets advanced and retreated over the last 120,000. From ETOPO1 data and sea level values, the total land area and land distribution change with time was calculated by spherical geometry using Matlab (matrix laboratory, a multi-paradigm numerical computing environment). The greatest change in aggregate terrestrial land area

occurred between 23.5° N and 66.5° N (12.6%), and 23.5° S to 23.5° N (15.6%). Over 56% of the aquaterra is located between equator and 66.5° N.

Acknowledgements

I would like to show my deepest gratitude to my advisor, Professor Jerome Dobson, committee members Stephen Egbert and Xingong Li, and all my friends in the Geography Department of the University of Kansas.

Table of Contents

List of Figures

List of Tables

1. Introduction and geographical history

1.1. Background

Global climate is linked inevitably to sea level. Whenever global temperatures fall, water shifts from oceans to ice sheets where it remains for long periods of time. When global temperatures rise, water is released back into the oceans. Thus, climate change is reflected as variations in ocean volume, which are global and termed 'eustatic' (Suess 1888). In this paper, I focus on long-term eustatic sea level change. For a better understanding, I refer to the landmass "aquaterra" – a distinctive global feature occupying the upper majority of the continental shelf and the lower fringe of the current coastal plain (Dobson 2014). This name emphasizes its unique character: for thousands of years it is covered by water (aqua) without interruption and for thousands of years it is exposed as land (terra). The most direct influence caused by sea level change is on coastal landforms and their human occupants. Human population distribution is not uniform on the Earth's landmasses (Small 1999). Analyses of sample study areas (Tokyo, New York, Bombay, Shanghai, Los Angeles, Calcutta, Buenos Aires, Seoul, Lagos, Osaka, and Rio de Janeiro) today show that most of the world's population is dispersed at low elevations close to coastlines rather than in large centralized cities, despite their high densities (Cohen 1998). Exploring aquaterra can inform studies of human and biophysical development

from ancient to modern times (Bailey and Flemming 2008). The timing of sea level change is important to our understanding of the dynamics of land area changes and their effects on the Earth's surface, especially physical and human development. Several main factors are responsible for long-term sea level change: water expands and contracts as it warms and cools; the amount of water contained as ice on land surfaces changes over time; in many places the continental shelf is dynamic, moving vertically due to eustatic pressures.

From the human perspective, when there are more choices for people to live and multiply, the capacity for development is higher. Geographical factors such as climate, water supply, and economics influence human development and settlement. The Earth's climate and global sea levels are closely linked to each other and, in turn, to human development and settlement. During cold periods some of the ocean's water is evaporated, precipitated, and then stored in ice caps or mountain glaciers, causing lower sea levels. During warmer periods sea levels rise as ice melts and add to the volume of the oceans. When sea level falls, more coastal land area is available for human occupation. Conversely, when sea level rises, less coastal land is available for human occupation. The 2007 (Intergovernmental Panel on Climate Change (IPCC)) report about the human impact of projected sea level rise found that 634 million people presently live in coastal areas vertically within 30 feet of sea level, and two thirds of the world's cities are located in these low-lying coastal areas. In

the past 20,000 years, much human progress and many cultural innovations occurred while seacoasts were quite lower than today.

Little is known about physical and human processes during the Late Pleistocene and Holocene ages. This time period is the same span during which modern human beings are known to have existed, and some studies have focused on the effects of glacial cycles on human development (Calvin 1990, Stringer and Gamble 1993). Now there is a crucial need for better understanding of climate change and risks associated with sea level rise in the coastal areas of today and the earlier ones of aquaterra. Mapping the relatively precise sequence of sea level rise and its associated effects on the detailed distribution of terrestrial lands can help scholars understand how the world responded to different sea level rises and falls. I plan to use global databases to compose an animation consisting of maps of ancient seacoasts through time and showing details of land area changes based on relevant attributes (latitude zones, longitude zones, etc.)

1.2. Sea Levels in the Late Pleistocene

Understanding sea level changes on land areas in different regions can give us an informed conception about how human populations developed. Sea level rises and falls caused the land area to be changing at least to some extent all of the time.

During the Last Glacial Maximum, ice sheets covered large areas in northern latitudes and global temperatures were significantly lower than today.

Paleo-records document significant changes in relative sea level (RSL). In order to understand the primary cause of this natural variability in sea level, we need to know what happened during the last deglaciation. Sea level at any location is a function of both the absolute elevation of the sea surface and vertical movements of the land, the balance producing a relative sea level. Uplift or subsidence of Earth's surface, vertical and horizontal motions of crust, and sediment compaction all can lead to local sea level change.

Major sea-level cycles occurred at intervals of approximately 100, 000 years (100ka) over the past approximately 800ka, with maximum amplitudes of 120–139 m. Smaller variations occurred with the major glacial and interglacial cycles. Global sea level has risen and fallen many times in response to advance and retreat of the Northern Hemisphere Ice Sheets that have dominated the last 2.5 Ma ("the Ice Ages"). Marine isotopic stages (MIS), sometimes referred to as Oxygen Isotope Stages (OIS), are the discovered traces of a chronological record of alternating cold and warm periods, going back at least 2.6 million years. With increased temperatures, the global ice volume declined, and far-field coral reefs recorded eustatic sea levels approximately 5–6 m higher than today at about 130,000 years ago (Lambeck and Chappell, 2001). I will start from about 120,000 years ago, when

the first fully modern humans appeared at the beginning of the Upper Pleistocene (Table 1.2.1).

Table 1.2.1 MIS stages and events

MIS Stage	Start Date	Cooler or Warmer	Cultural Events
MIS 1	11,600	Warmer	The Holocene
MIS 2	24,000	Cooler	Last glacial maximum, Americas populated
MIS 3	60,000	Warmer	Upper Paleolithic begins; Australia populated, upper Paleolithic walls painted, Neanderthals disappear
MIS 4	74,000	Cooler	Mt. Toba super-eruption
MIS 5	130,000	Warmer	Early modern humans (EMH) leave Africa to colonize the world
MIS 5a	85,000	Warmer	Howienson's Poort/Still Bay complexes in southern Africa
MIS 5b	93,000	Cooler	
MIS 5c	106,000	Warmer	EMH at Skuhl and Qazfeh in Israel
MIS 5d	115,000	Cooler	
MIS 5e	130,000	Warmer	

Recent assessments give an uncertainty of eustatic sea level at the LGM to a range of approximately 114 to 135 m (Shennan, 2007). Murray-Wallace (2007b) summarizes literature that suggests that during this time interval, sea level rose worldwide from approximately 120 to 130 m below present levels and almost attained (or in some locations exceeded) present levels by about 7ka.

Over the last 140,000 years sea level has varied over a range of more than 134 m. Paleo data from corals indicate that sea level was 4 to 6 m (or more) above present day sea levels during the last interglacial period, about 125,000 years ago. In the Last Glacial Maximum (LGM), roughly 24 and 19ka ago with largest ice sheets of the last glacial, sea level rose rapidly at average rates of about 10mm per year as the ice

melted, until about 6,000 years ago when the rates started to level off. Around 19,000 years ago, the ice sheets of North America and northern Europe began to melt. The meltwater from the ice sheets flowed into the oceans, raising sea level once again, and the land that had been beneath the ice began to rebound upwards, a process known as 'postglacial rebound' that is a local scale isostatic movement in Canada, Northern Europe, and Antarctica. Regarding future sea level change, the IPCC projects a rise between 0.09 m and 0.88 m by 2100 (Houghton et al., 2001).

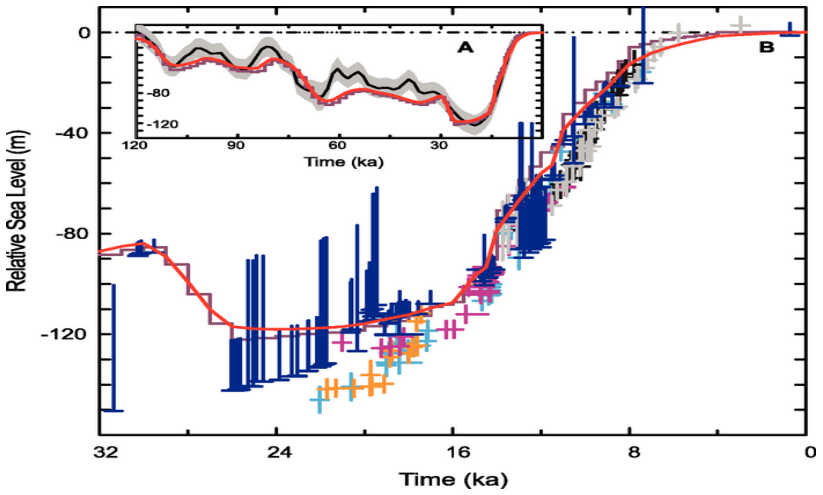

Figure 1.2.1 Relative sea level change through the past 32,000 years

Table 1.2.2 An overview of human developments over the past 100,000 years

More than 100,000 years	100,000 B.P.	90,000 B.P.	80,000 B.P.	70,000 B.P.	60,000 B.P.	50,000 B.P.	40,000 B.P.	30,000 B.P.	20,000 B.P.	10,000 B.P.
End of Pleistocene	Early Homo sapiens diet	People used bone tools and lived on seafood in the South African coast dating to 70,000 years before present (BP) according to cave discoveries.				Extinctions of mammals and birds in Australia.	Cave paintings, stone tools in most of Europe.	European early modern humans (EEMH) thriven in cold European climate.	Global temperature averages 8 degrees C cooler.	Estimated 5 million Homo sapiens lived.

Past 10,000 years	10,000 B.P.	9,000 B.P.	8,000 B.P.	7,000 B.P.	6,000 B.P.	5,000 B.P.	4,000 B.P.	3,000 B.P.	2,000 B.P.	1,000 B.P
Agriculture and Technology development	First evidence of plant domestication.	Flax used for clothing in Syria and Turkey.	Beans planted in eastern Mediterranean.	Squash, beans and corns appeared in Americas.	Cotton grown in Pakistan.	Soybeans, rice, wheat, millet and barley used in China.	Olives, peaches cultivated in eastern Mediterranean.	People started to sail.		About 250 – 345 million Homo sapiens on planet.

1.3. Human Population Distributions

From reviewed literatures, there are two models of early modern human colonization of Eurasia in the Upper Pleistocene: (i) from multiple *Homo sapiens* source populations that had entered Arabia, South Asia, and the Levant prior to and soon after the onset of the Last Interglacial (MIS-5), (ii) from a rapid dispersal out of East Africa via the Southern Route (across the Red Sea basin), dating to ~74–60ka. Historical human migration began about 1.8 million years ago when the pre-modern Homo erectus moved out of Africa across Eurasia. The ancestor of the human species H. sapiens evolved into Modern Humans around 200,000 years ago in Africa. "Modern humans" are defined as the *Homo sapiens* species, of which the only extant subspecies is known as *Homo sapiens*. Migrations of Modern Humans out of Africa occurred around 125,000 years ago according to Arabian archaeological finds of tools in the region when sea levels were higher even than today. They reached the Near East from East Africa across the Bab al-Mandab Strait and the Arabian Peninsula.

The human population growth curve during the Late Pleistocene is J-shaped, and is accelerating through time (Figure 1.2). In the relationship between land cover and human development, carrying capacity per unit area is an important factor. Carrying capacity is defined as the maximum number of individuals of a given species that a given environment can sustain indefinitely, given the food, habitat, water and other necessities available.

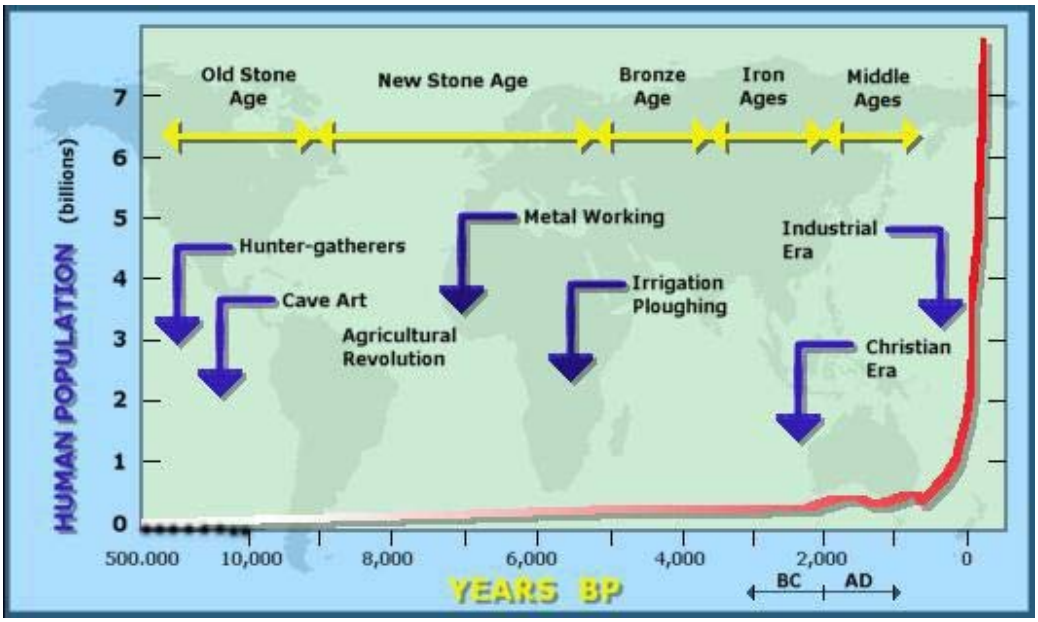

Figure 1.3.1 Human population growth over time

Land changes in many ways over time, each parcel varying greatly in terms of elevation, climate, and other variables such as distance from the sea. I plan to classify each 1 arc second cell based on different latitudes and longitudes. Dobson (2014) measured aquaterra in three major latitudinal groups — tropical (38 percent), mid-latitude (44 percent), and Arctic/Antarctic zones (18 percent). I will

address the four main factors affecting local climate: latitude, topographic relief (altitudinal zonation, orographic uplift, and rain shadow effects), major wind patterns, and distance from the sea (continental vs. maritime). Human cultural development is closely tied to changes in the natural environment. Figure 1.2 presents the historical record (not adjusted for land area), typical of a "J-shaped" growth, with humans filling new niches and (perhaps) not yet reaching a limiting carrying capacity.

1.4. Research Questions

The name ‘aquaterra’ refers to the lands that were alternately exposed and inundated as ice sheets advanced and retreated over the last 120,000 years (Dobson 2014). This period consists of two epochs, Late Pleistocene and Holocene. First, I plan to provide a clear view of how eustatic sea level varies globally through time. Using best available sea level records according to Marine isotopic stages (MIS) stages, I will calculate the horizontal global sea level change curve through time. Using geographic information system (GIS) software, I will map the results in order to visualize the seacoast change and the areal extent of exposed portions of aquaterra at intervals of one thousand year. Based on the curve I will produce a series of world maps of ancient seacoasts that can be incorporated into an animation over time.

Based on the sea level change curve interpolated from original *in situ* data available in scientific literature, I will emphasize those extreme changes in the global distribution of aquaterra. Also I will use trend analysis methods to see if there is a periodic pattern or linear changing trend for sea level change in the last 120,000 years. In order to understand land area change, hypsographic change caused by sea level change is needed. Hypsographic change deals with the measurement and mapping of the varying elevations of the earth's surface above sea level. Finally, I will simulate land distribution changes at the land-sea interface.

2. Data source

2.1. Sea level data

Historical sea level depths data are collected from numerous sites using different sea-level indicators around the world (Lambeck and Chappell 2001; Yokotama et al 2000; Peltier and Fairbanks 2006; Siddall, M., et al. 2006). Many are expressed as glaciers and ice sheets volume equivalent sea level data (Nakada and Lambeck 1988; Fleming et al. 1998; Chappell and Shackleton 1986). Dating of coral reef terraces provides a good record of *in situ* changes in sea level. As massive weights of water shift, changes in eustatic pressure, in turn, cause uplifting and subsidence of land, a local phenomenon that must be taken into account. Hence, most studies begin with searching for stable sites likely unaffected by uplifting and subsidence. Oxygen isotope ratios provide a potential means for reconstructing sea level change over the past 100 Myr. Below is a table showing different published sea levels of the Last Glacial Maximum. The lowest values range from 105 to 145 meters below current global sea level due to different databases they used.

Table 2.1.1 Published Sea-level values of the LGM

Reference	Sea level (m)	Location or method
Veeh and Chappell 1970	120	Huon Peninsula, up. Coral
Carter and Johnson 1986	114-133	the Great Barrier Reef, sed
Chappell and Shackleton 1986	130	$\delta^{18}O$
Nakada and Lambeck 1988	130	Isostatically corrected data from intermediate- and far-field
Fairbanks 1989, Bard et al 1990	117	Barbados, dr. Coral
Tushingham and Peltier 1991	115	Isostatically corrected data mainly from near- and intermediate-field
Peltier 1994	105	Data from Barbados corrected for isostasy but not for tectonics
Ferland et al 1995	< 130	Off Sydney, sed
Colonna et al 1996	145	Mayotte, sub. Coral
Fleming et al 1998	125	Isostatically and tectonically corrected data from intermediate- and far-field

δ^{18}□: Foraminiferal $\delta^{18}O$ record obtained from deep-sea sediment core; sed: sediment core taken from sea floor; up.Coral: uplifted coral reefs; dr.Coral: drilled coral obtained from offshore; sub.Coral: coral obtained by submergible from sea floor.

Global mean sea level has been measured as mean distance of the ocean surface above the center of the Earth. Many proxies found in deep-sea sediments including trace metal and isotopic composition of fossil plankton, species composition, and lithology can be interpreted as sea level indicators.

There are more historical records for the LGM interval. Drilling into tropical coral reefs (Fairbanks 1989; Peltier and Fairbanks 2006; Lambeck and Chappell 2001) often yields relatively continuous sea level records. Such records have provided high-precision dates based on U-Th dating that are not subject to the uncertainties of reservoir and calendar age corrections.

When conducting the RSL data from different sites during deglaciation, one must consider that the ocean basins are growing larger since the end of the last cycle of glaciation. Glacial isostatic adjustment (GIA) is needed to when comparing site records.

Figure 2.1.1 below shows the sites I employed to interpolate global sea level change.

Figure 2.1.1 Sites: West Australia, Huon Peninsula, Oahu, Tahiti, Cayucos, Oregon, California, Florida Keys, Grand Cayman, Bermuda, Barbados, Red Sea.

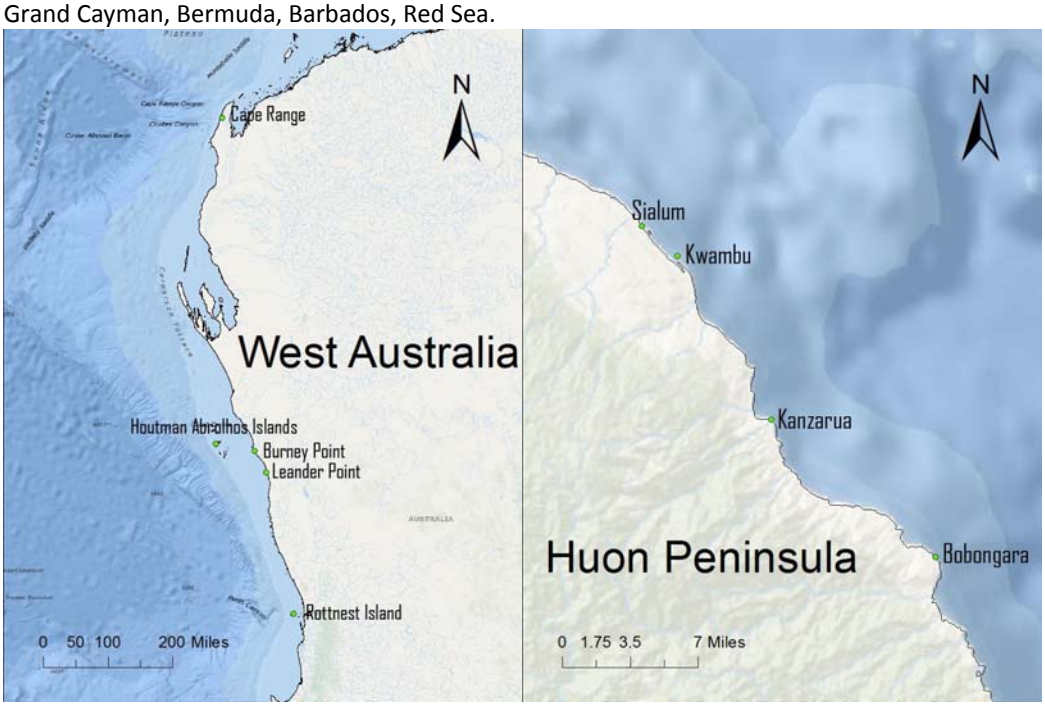

a b


N
Kahuku Point
Ka'ena Point
Ka'ena Point State Park
Oahu
Mokapu Point
Ala'ala Point
Kahe Point
0 3.5 7 14 Miles

c

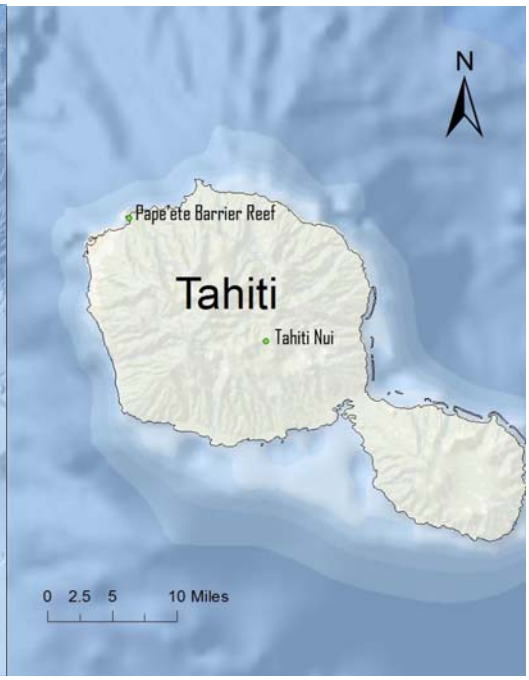
N
Pape'ete Barrier Reef
Tahiti
Tahiti Nui
0 2.5 5 10 Miles

d


N
Coquille Point
California and Oregon
Point Arena
Cayucos
Palos Verdes Hills
San Nicolas Island
0 62.5 125 250 Miles

e

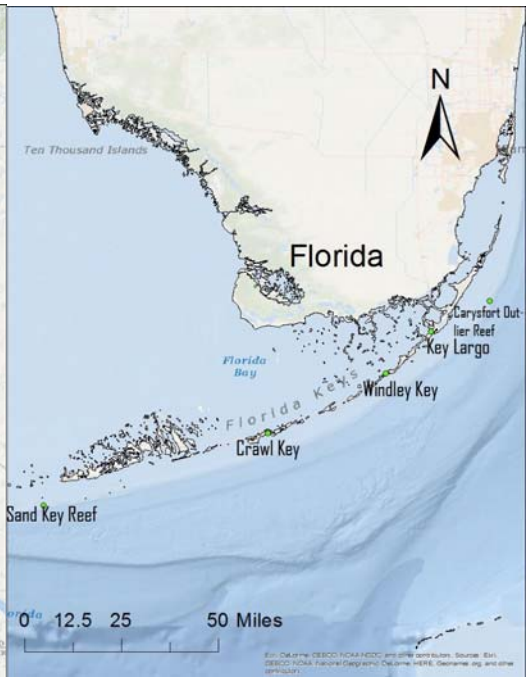
N
Ten Thousand Islands
Florida
Carysfort Outlier Reef
Key Largo
Florida Bay
Florida Keys
Windley Key
Crawl Key
Sand Key Reef
0 12.5 25 50 Miles

f

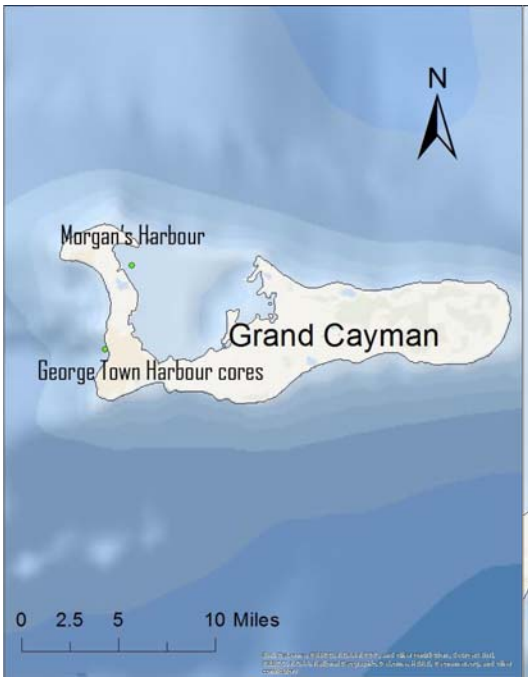
N
Morgan's Harbour
Grand Cayman
George Town Harbour cores
0 2.5 5 10 Miles

g

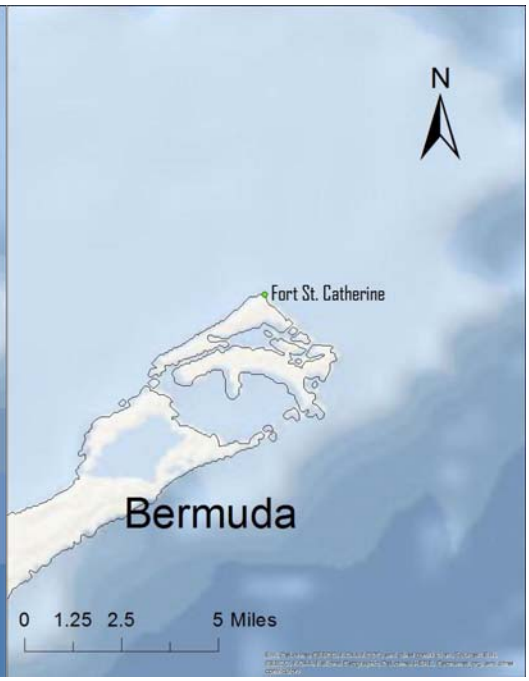
N
Fort St. Catherine
Bermuda
0 1.25 2.5 5 Miles

h


N
Barbados
Cave Hill
First High Cliff
Salt Cave Point
South Point
0 2.5 5 10 Miles

i


N
North Aegean Trough
Aegean Sea
Aegean Sea
0 15 30 60 Miles

j

Figure 2.1.2 Detailed site maps: a to j: west Australia, Huon Peninsula, Oahu, Tahiti, Cayucos, Oregon, California, Florida Keys, Grand Cayman, Bermuda, Barbados, Red Sea

a. The western passive margin of Australia is thought to be tectonically stable during the late Pleistocene, and thus fossil reefs there can provide decisive information about the timing of sea level change. This place is located far from the former penultimate glacial maximum ice sheets. Thorium and its isotopes are measured for dating the corals. Samples were collected from Rottnest Island, Leander Point, Houtman Abrolhos Islands, Burney Point, and Cape Range (Ref.65, 66,83). The first two samples were from in-situ coral with the Rottnest Limestone and the fossil reef complex.

b. The spectacular uplifted coral terraces of Huon Peninsula on Papua New Guinea's north coast are an iconic location for sea-level studies. Huon lies at the tectonically active junction of the Australian and Pacific plates. It is surrounded by emergent coral terraces that contain a good record of historic change for about 250ka. Exposed coral reef samples were collected near Kwambu, Kilasario, Kanzarua, and Kanomi. Drill-core samples were collected near Kwambu in 1996 and Kanomi and Gagidu Point in 1997. Other coral samples were collected from terrace complex at Bobongara and Aladdin's Cave (Chappell, 1974; Aharon et al., 1980; Aharon and Chappell, 1986; Ota and Chappell, 1999) (Ref.13, 19, 23, 80).

c. Oahu is a part of the Hawaii-Emperor volcanic seamount chain that stretches more than 5,800 kilometers (3,600 miles) from the Aleutian Trench in the far

northwest Pacific to the Loʻihi. Oahu is the third largest island in the archipelago. Six Waimanalo Formation (23 million years ago) coral localities are chosen (Alala Point; Mokapu Point; Kahuku Point; East Kaena Poiny Reef; Kaena Point State Park; Kahe Point). These corals from slowly uplifting Oahu range from 110 to 134ka, with most ages between 115 to 125ka (Ref.68, 51).

d. The island of Tahiti (French Polynesia) is a hot-spot volcanic island that has a slow subsidence rate. It is a far-field site located far from large ice sheets and major isostatic rebound effects. Submerged data were collected by the Integrated Ocean Drilling Program (IODP) Expedition 310 and onshore of the Papeete barrier reef (Ref. 69).

e. The lower terrace in the Cayucos located in San Luis Obispo County, California is geomorphically exposed. Boulders overlaid by fossiliferous sands and coquina compose into marine deposits on the platform. Two fossil localities (10731 and 11923) were selected because they have abundant corals. Uranium-series analyses of corals records show an open-system history (Ref. 52).

On the Pacific Coast of North America, there are eight coral sampling localities in California and one in Oregon. They were selected to study precise timing and palaeoclimatic aspects of the high sea level events. All sites are marine terrace localities and deep-sea core locations. The coral deposit collected is a solitary

species, B. *elegans*, which is most common along the marginal eastern Pacific Ocean (Ref. 53).

f. Florida is an advantageous region to estimate past high sea levels because (1) South Florida is tectonically stable; (2) the Florida Keys are not on any volcanic hot spot chain and therefore no uplift due to lithospheric loop, and (3) South Florida has a favorable environment for coral reefs to grow and develop. Several localities, one near Sand Key Reef mainly consist of coral *Montastrea annularis*; one on Crawl Key, one on Key Largo; and, one on Windley Key. The Key Largo Limestone, a fossil coral reef exposed at the surface in the Florida Keys, and the Miami Limestone, consists of an oolitic facies and a bryozoan facies recording the last interglacial sea levels (Ref. 46, 50, 73). The ages of the corals are dated by U-series and TIMS.

g. Grand Cayman, one of the Cayman Islands that are outcrops of the Cayman Ridge, is located in the northwest part of the Caribbean Sea. Although these islands are located in a tectonically active area with a spreading center and close to the Oriente Transform fault, Grand Cayman is considered to be tectonically stable (Jones and Hunter 1990). Nine offshore corals from George Town and two onshore corals located on the western part of the island were collected in the Ironshore Formation on Grand Cayman (Ref. 17). This formation, defined by Matley (1926), consists of poorly consolidated limestones that commonly contain reef faces, bivalves,

gastropods, and calcarenites. The offshore samples were analyzed by thermal ionization mass spectrometry (TIMS).

h. Bermuda is located on the Mid-Atlantic Ridge (MAR), created by volcanic eruptions 123 to 124 million years ago. About 1-2 million years ago, the top of the volcanic seamount was eroded down below sea level and corals began to grow around the margins. Fossil *Oculina* corals, one type of eolianite unit called the Southampton Formation, were collected for dating at Fort St. Catherine, which is distant from plate boundaries (Ref.46). High-precision TIMS U-series dating method was used to get the ages.

i. The island of Barbados is located in the eastern Caribbean Sea, situated east of the ridge of the Lesser Antilles magmatic arc platform and above the active subduction zone between the Atlantic Oceanic lithosphere of the South American Plate and the overriding Caribbean Plate. Samples were collected from the Barbados II terrace (Ventnor terrace), Barbados I terrace (Worthing terrace), Holders Hill, Grazettes Quarry, West Indies hill, and Rendezvous Hill terrace at Cave hill (Ref. 6, 19, 26, 30, 56, 63, 70). The extended coral-based RSL curve from the island of Barbados in the Caribbean Sea (Fairbanks, 1989; Peltier and Fairbanks, 2006) is especially important, as the RSL history from this site has been shown to provide a good approximation to the ice-equivalent eustatic curve itself (Peltier, 2002).

j. Red Sea sea level data are transferred from an eastern Mediterranean core LC21 by correlating its $\delta^{18}O_{ruber}$ record with the Soreq Cave$\delta^{18}O_{speleo}$. LC21 was recovered from the SE Aegean Sea, on the boundary between the north-south extended Aegean Sea and the west-east extended Levantine Sea (Ref.35). The analysis of the Red Sea O isotopic record by Siddal et al. (2003) further supports the validity of the interpretation of the extended Barbados record by Peltier and Fairbanks (2006).

Table 2.1.2 situ data temporal resolution and sea level range

Sites	Relative sea level (m)	Time	**Sites**	Relative sea level (m)	Time
West Australia	-23.5 – 3.3	4 – 125ka	California	-20.3 – 6.3	75 – 123ka
Huon Peninsula	-111.1 – 6.1	12 – 122ka	Florida keys	-22.7 – 5.3	81–125ka
Oahu	-3.3 – 6.0	110–125ka	Grand Cayman	1.0 – 6.0	5 – 124ka
Tahiti	-130.1--32.8	9 – 65ka	Bermuda	1.5	77 – 83ka
Cayucos	5.8 – 6.5	109-125ka	Barbados	-150.5 – 6.1	7 – 125ka
Oregon	-20.7--18.4	78 – 82ka	Red Sea	-108.08-10.25	0 – 125ka

2.2. Global land topography and ocean bathymetry data

2.2.1. Digital Elevation Model (DEM) data

ETOPO1 is a 1 arc-minute global relief model of the Earth's surface (Amante and Eakins 200, Eakins and Sharman 2012) that is produced by the National Oceanic and

Atmospheric Administration (NOAA) from satellite altimetry and ship-based sonar soundings (Smith and Sandwell 1997). The study area covers latitudes between -90° to +90° worldwide. Its hypsometry integrates land elevation and ocean bathymetry. The horizontal datum of ETOPO1 is WGS 84 geographic and the vertical datum of ETOPO1 is sea level. The vertical accuracy of ETOPO1 is 10 meters at best. Below is an Ice Surface image that depicts the surface of the Antarctic and Greenland ice sheets.

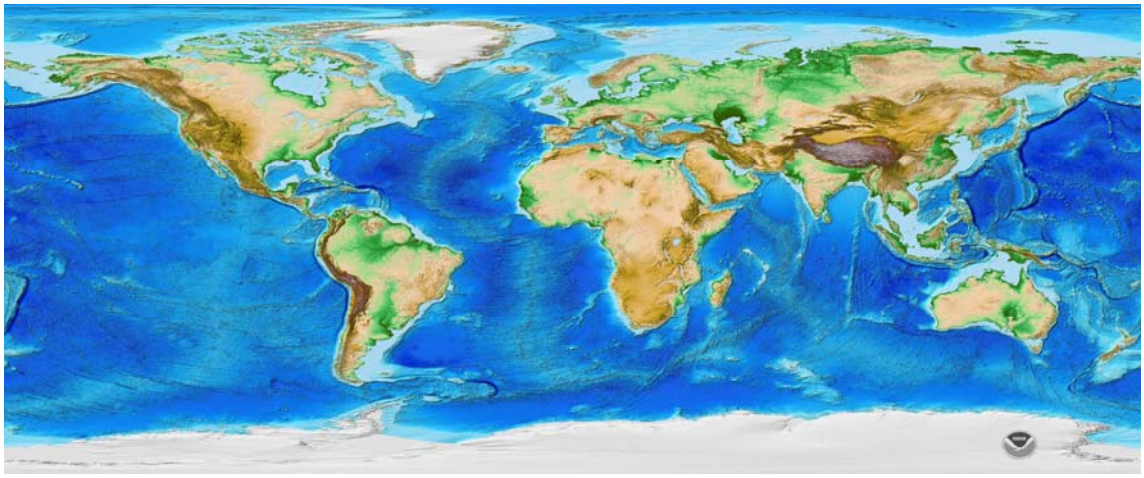

Figure 2.2.1.1 Color shaded-relief image of Earth from ETOPO1 Ice Surface (National Geophysical Data Center (NGDC))

2.2.2. Global Shoreline

Global Self-consistent Hierarchical High-resolution Shorelines (GSHHS) (Wessel and Smith, 1996) is a high-resolution shoreline data set from the World Data Bank II (WDB; also known as CIA Data Bank) [Gorny, 1977], which has coastlines, lakes, boundaries, and rivers, and the World Vector Shoreline (WVS) database [Soluri and Woodson, 1990], which only contains shorelines along the ocean/land interface. It

has 4 hierarchical levels: boundary between land and ocean (L1), boundary between lake and land (L2), boundary between island-in-lake and lake (L3), and boundary between pond-in-island and island (L4). I used L1 and L2 to justify inland water bodies' area because the pond areas are quite small.

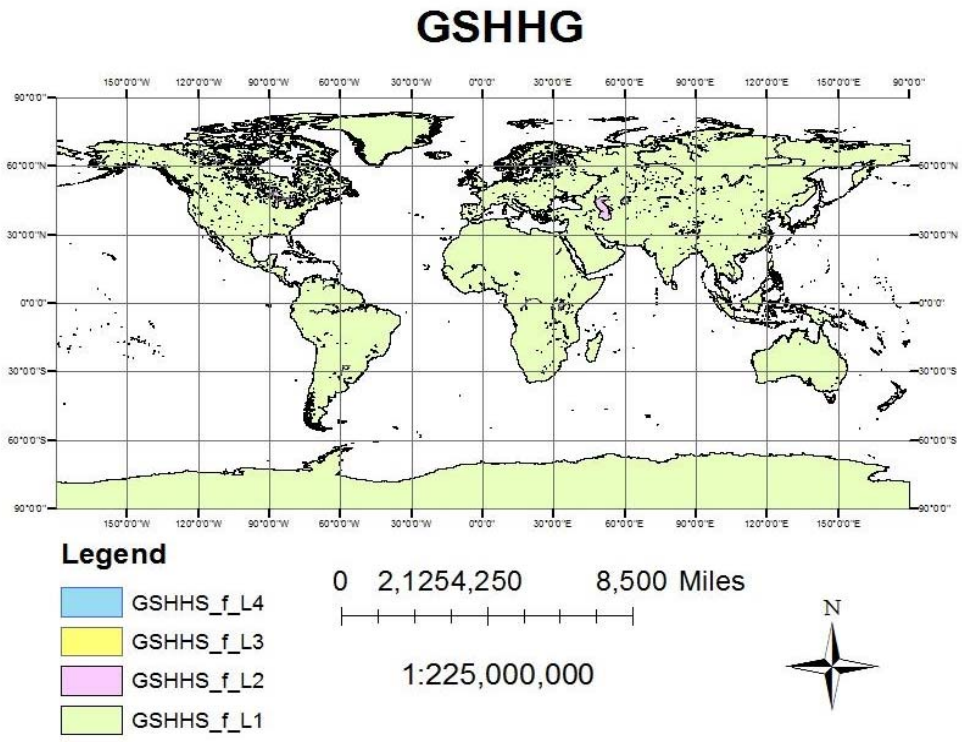

Figure 2.2.2.1 Global Self-consistent Hierarchical High-resolution Shorelines (full resolution) map

3. Methods and techniques

3.1. Nonlinear Regression

Based on the physical data sets from these sites, I assume there is a spatial and temporal function f (x) that passes through all data points and also represents the variable of interest at all non-data points, including the original data set. In order to get a good fit or a best fit to the original data, I need to apply curve fitting to create a new function that does not have to pass through the original data set. There are many interpolation methods one can use: piecewise constant linear interpolation, which simply connects each data point with a straight line; smoothing and filtering noisy data with local regression; or a sum of sine and cosine function that describes a periodic signal.

I chose to use the Matlab curve fitting toolbox and program to fit and interpolate all site data. Basically, curve fitting builds a model that has a single input and single output (SISO). For regression models, linear regression and nonlinear regression are two basic approaches. Test results of different models, according to the variation of climate during the last 120,000 years, select the most reasonable model to predict the sea level data. The sea level data are non-uniform and nonlinear distributed; thus linear regression and interpolation (nearest neighbor, cubic spline) are not suitable for analysis.

Curve Fitting Toolbox software uses the nonlinear least-squares formulation to fit a nonlinear model to a data distribution. A nonlinear model is defined as an equation that is nonlinear in its coefficients or is a combination of linear and nonlinear in its coefficients. For example, Gaussians, ratios of polynomials, and power functions are all nonlinear.

3.1.1. Fourier Series

French scientist and mathematician Jean Baptiste Fourier (1768–1830) proved the mathematical fact that any periodic waveform can be expressed as the sum of an infinite set of sine waves. The sea level data are approximately periodic, which suggests that they can be described by Fourier series. The Fourier series model is a sum of sine and cosine functions that describes a periodic signal. This is the trigonometric Fourier series form:

$$y = a_0 + \sum_{i=1}^{n} \quad a_i cos\,(iwx) + b_i\, sin\,(iwx) \tag{3.1}$$

where a_0 (direct current term) models a constant term in the data and is associated with the i=0 cosine term, w is the fundamental frequency of the signal, n is the number of terms in the series, and $1 \ll n \ll 8$. The two expressions after the Σ signs are the Fourier coefficients of the function f (t).

To obtain the coefficient estimates of the fitting process, the least-squares fitting method minimizes the summed square of residuals. The residual for the ith data

point r_i is defined as the difference between the observed response value y_i and the fitted response value $\hat{y}_i$, and is identified as the error associated with the data.

$$r_i = y_i - \hat{y}_i \tag{3.2}$$

residual=data−fit

The summed square of residuals is given by

$$S = \sum_{i=1}^{n} r_i^2 = \sum_{i=1}^{n} (y_i - \hat{y}_i)^2 \tag{3.3}$$

where n is the number of data points included in the fit and S is the sum of squares error estimate.

Least-squares fitting is sensitive to extreme values called outliers. There are two robust regression methods: least absolute residuals (LAR), and bisquare weights. The bisquare weights method minimizes a weighted sum of squares, where the weight given to each data point depends on how far the point is from the fitted line. Points near the line get full weight. Points farther from the line get reduced weight. For most cases, the bisquare weight method is preferred to LAR because it simultaneously seeks to find a curve that fits the bulk of the data using the usual least-squares approach, and it minimizes the effect of outliers.

Robust fitting with bisquare weights uses an iteratively reweighted least-squares algorithm, and follows this procedure:

1. Fit the model by weighted least squares.

2. Compute the adjusted residuals and standardize them. The adjusted residuals are given by

$$r_{adj} = \frac{r_i}{\sqrt{1-h_i}} \tag{3.4}$$

r_i are the usual least-squares residuals and h_i are leverages that adjust the residuals by reducing the weight of high-leverage data points, which have a large effect on the least-squares fit. The standardized adjusted residuals are given by

$$u = \frac{r_{adj}}{K_s} \tag{3.5}$$

K is a tuning constant equal to 4.685, and s is the robust variance given by MAD/0.6745 where MAD is the median absolute deviation of the residuals.

3. Compute the robust weights as a function of u. The bisquare weights are given by

$$w_i = \{(1-(u_i)^2)^2,\ |u_i| < 1\ 0,\ \ |u_i| \geq 1 \tag{3.6}$$

4. If the fit converges, finish the fitting progress. Otherwise, perform the next iteration of the fitting procedure by returning to the first step.

According to the values of the coefficients and the goodness-of-fit, the best fitting result has 8 terms; Robust is set to bisquare method that reduces the weight of outliers.

3.1.2. Sum of sine

This model fits periodic functions as does Fourier Series, and is given by

$$y = \sum_{i=1}^{n} \quad a_i sin\,(b_i x + c_i) \tag{3.7}$$

where a is the amplitude, b is the frequency, and c is the phase constant for each sine wave term. n is the number of terms in the series and $1 \ll n \ll 8$. The difference from Fourier Series is that the sum of sines equation includes the phase constant, and does not include a constant (intercept) term.

The number of terms is set to highest to improve the fit quality. Robust is set to bisquare. The Center and scale option can be used when there are dramatic differences in variable scales or the distance between data points varies across dimensions.

3.2. Smoothing

This is a nonparametric method of smoothing (drawing a smooth curve trough noisy observations) using a spline function which can be piecewise-defined by polynomial functions. The smoothing spline s is constructed for the specified smoothing parameter p and the specified weights w_i. The smoothing spline minimized

$$p \sum_i \quad w_i(y_i - s(x_i))^2 + (1-p) \int \quad (\frac{d^2 s}{dx^2})^2 dx \tag{3.8}$$

if the weights are not specified, they are assumed to be 1 for all data points. When p = 0, a least-square straight-line is produced to fit the data, while p = 1 produces a cubic spline interpolant. In this case, the smoothing parameter p is set to 0.995. Also, since sea level data collected from different sites typically have different time scales, it is better to normalize the inputs (predictor data) when there are dramatic differences in variable scales or when the distance between data points varies across dimensions. In Matlab the option would be center and scale.

3.3. Measurement of central tendency

A measure of central tendency is a single value that attempts to describe a set of data by identifying the central position within that set of data. The three most common measures of central tendency: the mean, the median, and the mode. The mean (or average) is the most popular and well-known measure of central tendency. However it is very sensitive to outliers. The median and the mode are the only

measures of central tendency that can be used for ordinal data. When a set of data has outliers or skewers, extreme values do not affect median and mode as strongly as they do the mean. The mode may be than one answer and is every value when no values repeat.

3.4. Mann-Kendall Trend Test

Mann-Kendall (MK) test is used in trend-detection studies of hydrological time series by many researchers. For a time series data sample, a time series plot can initially determine whether the data values are randomly distributed, or have some patterns or trends. The original purpose of the Mann-Kendall (MK) test (Mann 1945, Kendall 1975, Gilbert 1987) was to see if there is a monotonic upward or downward trend over time. A monotonic trend means there are consistent increases or decreases, but the trend may not be linear.

The Mann-Kendall (MK) Trend Test is a nonparametric test, which does not require normally distributed data. The global sea level change trough time may not have a trend or has different trends in different time periods. Here is how the MK test works (Gilbert 1987):

List data over time, $x_1, x_2, \dots, x_n$, determine the sign of all $\frac{n(n-1)}{2}$ possible differences $x_j - x_k$, where j >k,

1. Let the sign be an indicator function, that is,

$$\operatorname{sgn}(x_j - x_k) = \begin{cases} 1 \; if \; x_j - x_k > 0 \\ 0 \; if \; x_j - x_k = 0 \\ -1 \; if \; x_j - x_k < 0 \end{cases} \tag{3.12}$$

2. Calculate

$$S = \sum_{k-1}^{n-1} \quad \sum_{j-k+1}^{n} \quad sgn(x_j - x_k) \tag{3.13}$$

if S is a positive number, observations collected later in time tend to be larger than earlier ones, and vice versa. The Kendall τ coefficient is defined as:

$$\tau = \frac{s}{\frac{1}{2}n(n-1)} \tag{3.14}$$

(1) If the agreement between the observations and time is perfect (i.e., the observations have the same rankings with time), τ has a value of 1.

(2) If the disagreement between the observations and time is perfect (i.e., observations have reverse rankings with time), τ has a value of −1.

(3) If X and Y are independent, then one would expect the coefficient to be approximately zero.

3. In this case, n is greater than 8 (Mann, 1945; Kendall, 1975), the statistic S is approximately normally distributed with the mean and the variance as follows:

$$VAR(S) = \frac{1}{18}[n(n-1)(2n+5) - \sum_{p-1}^{ng} \quad t_p(t_p-1)(2t_p+5)] \tag{3.15}$$

$E(s) = 0$

where g is the number of tied groups and t_p is the number of observations in the p^{th} group.

4. If the residuals are independent, use standardized test statistics Z value as follows:

$$Z = \begin{cases} \frac{S-1}{\sqrt{VAR(S)}} \; if \; S > 0 \\ 0 \; if \; S = 0 \\ \frac{S+1}{\sqrt{VAR(S)}} \; if \; S < 0 \end{cases} \tag{3.16}$$

a positive Z means the data tend to increase with time; a negative Z means the data decrease with time.

5. From the Z value, the probability p-value can be obtained using the formula below (Yue et al., 2002):

$$P = \frac{1}{\sqrt{2\pi}} \int_{-\infty}^{Z} \quad e^{-\frac{t^2}{2}} \, dt \tag{3.17}$$

For independent observations without trends the P value should be equal to 0.5, for a large positive trend the P value should be close to 1, and for a large negative trend the P value should be close to 0.

Under the influence of some climate cycles, hydrological and climatic data may have a regular trend within a period of time. Since sea level would be affected by ice volume change driven by climate change, the sea level change may have similar cycles. In order to reduce the possibility of being misled by autocorrelation while doing the Mann-Kendall test, a pre-whitening or variance correction method can be used to eliminate the effect of serial correlation. Pre-whitening is applied to remove (or rather to reduce) the auto-correlation part before doing a trend test, and it can remove part of the magnitude. Various models can be used in pre-whitening such as an autoregressive model, moving average model (Hamed and Rao, 1998), or combined model.

The common pre-whitening procedure will lead to potentially inaccurate assessments of the significance of a trend when testing on serial correlation data. Yue et al. (2002) proposed a trend-free pre-whitening (TFPW) procedure to eliminate the effect of autocorrelation. The TFPW Mann-Kendall test can be explained as below:

1. Remove the influence of lag-one autoregressive (AR(1)) component, r_1:

$$Y_t = X_t - r_1 X_{t-1} \quad (3.18)$$

where r_1 is given by: $r_1 = \frac{\sum [Y_t - E(Y_t)][Y_{t-1} - E(Y_t)]}{\sum [Y_t - E(Y_t)]^2}$,

2. Put the new data back in the series:

$$Y_t' = Y_t + bt \quad (3.19)$$

Apply the MK test to the new series above, where b, the slope of the trend is estimated using the TSA (Theil, 1950a–c; Sen, 1968), is an estimate of the magnitude trend:

$$b = Median(\frac{X_j - X_l}{j - l}) \forall l < j \quad (3.20)$$

3.5. Calculate land area change through time

The National Geophysical Data Center (NGDC) has plotted the distribution of elevations and cumulative elevations of the Earth's surface with its Ice Surface global relief model. A hypsographic curve describes an area as a function of submerged depth (bathymetry) or terrestrial height (elevation). It is a cumulative height frequency curve for the Earth's surface or some part thereof.

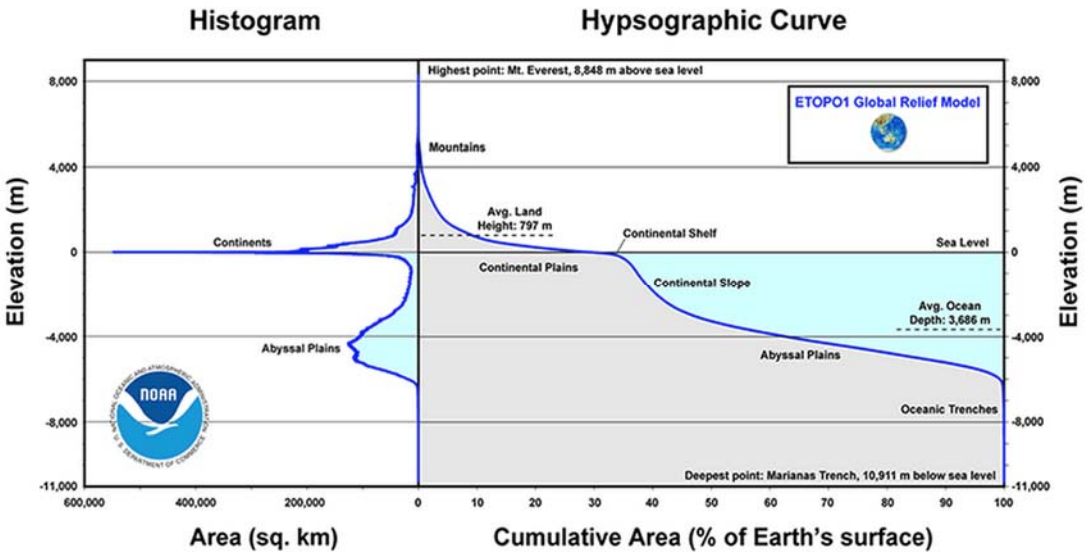

Figure 3.5.1Global histogram and hypsographic curve of Earth's surface (Ref.22)

This histogram was determined using the equation below to calculate the area of each cell,

$$dA = a^2 cos\,[\phi(1-e^2)]\,d\phi dl/(1-e^2 sin^2\phi)^2 \qquad (3.21)$$

where:

Latitude (ϕ) = latitude of cell's center (in radians)

Unit of Latitude ($d\phi$) = 1 arc-minute (0.0166667 degrees)

Unit of Longitude (dl) = 1 arc-minute (0.0166667 degrees)

The WGS84 spheroid was used for values of the Earth's radius and eccentricity:

Equatorial radius (a) = 6378.137 km

Eccentricity (e) = 0.08181919

The Earth is considered as an ellipsoid and the coordinate system WGS 84 is used in calculating ice surface area. The WGS 84 datum surface is an oblate spheroid (ellipsoid) with major (equatorial) radius a= 6378.137 km at the equator and flattening f=1/298.257. Any irregular polygon can be considered as a union of many triangles. When calculating the area change through time, I use spherical geometry to deal with different zones' calculations.

1. When the area is a rectangle in the whole 360 degree zone, the area between two lines of latitude is the difference between the area north of one latitude and the area south of the other latitude:

$$A = |2\pi R^2(1 - sin\,(lat2)\,) - 2\pi R^2(1 - sin\,(lat1)\,)| \\ = 2\pi R^2|sin\,(lat1) - sin\,(lat2)\,| \qquad (3.22)$$

The area of a lat-long rectangle is proportional to the difference in the longitudes. So the area change is:

$$A = A * |lon\dot{1} - lon2|/360$$

2. When the area is a triangle (shown as below),

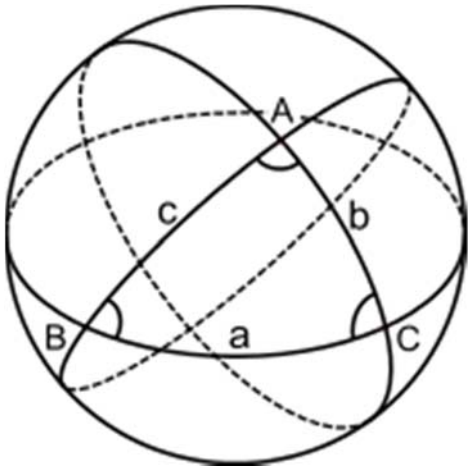

the area on the surface of the sphere of radius R is given by the formula:

$$A = \frac{\pi R^2 E}{180^o}$$

where E is the amount by which the sum of the angles exceeds π radians in degrees called the spherical excess. Spherical excess can be defined as:

$$E = A + B + C - 180^o \tag{3.23}$$

$$\text{or } tan\ \tfrac{1}{4}\ E = \sqrt{tan\ \tfrac{1}{2} s\ tan\ \tfrac{1}{2}(s-a) tan\ \tfrac{1}{2}(s-b) tan\ \tfrac{1}{2}(s-c)} \tag{3.24}$$

where $s = \frac{1}{2}(a + b + c)$.

4. Results and interpretation

4.1. Global sea level fitting

All sea level data are non-uniformly distributed through time and some of them have overlap with each other. When running sea level interpolation, the challenge is to join all data points into one continuous time series dataset. Below is a brief view of all data acquired for my analysis:

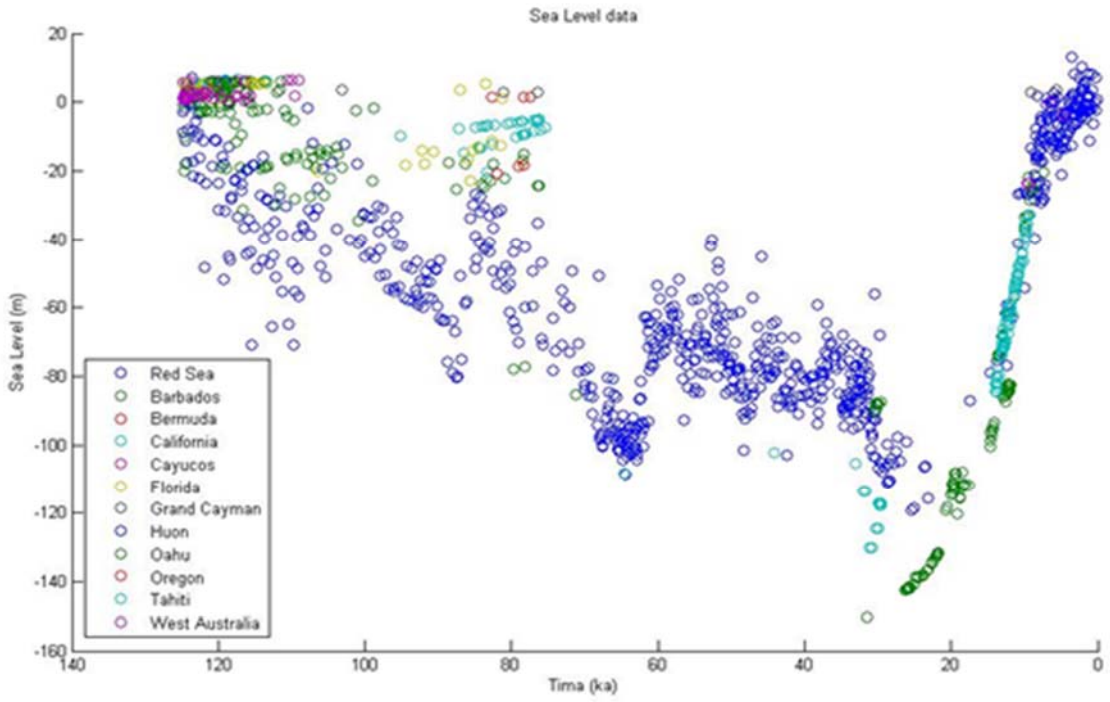

Figure 4.1.1 Sea level data for the past 120,000 years

I used the Matlab curve fitting function to generate all these data points, which are sorted through time and two equations for the Fourier series and Sum of Sine fit functions.

Here is the fit function of the Fourier series:

f(x) = a0 + a1*cos(x*w) + b1*sin(x*w) +

a2*cos(2*x*w) + b2*sin(2*x*w) + a3*cos(3*x*w) + b3*sin(3*x*w) +

a4*cos(4*x*w) + b4*sin(4*x*w) + a5*cos(5*x*w) + b5*sin(5*x*w) +

a6*cos(6*x*w) + b6*sin(6*x*w) + a7*cos(7*x*w) + b7*sin(7*x*w) +

a8*cos(8*x*w) + b8*sin(8*x*w)

Coefficients (with 95% confidence bounds):

a0 = -50.84 (-52.95, -48.72)

a1 = 15.63 (3.904, 27.35), b1 = -39.5 (-42.67, -36.34)

a2 = 13.17 (4.552, 21.79), b2 = -11.91 (-13.9, -9.917)

a3 = 12.79 (-0.5827, 26.16), b3 = -7.775 (-13.69, -1.858)

a4 = 3.866 (-12.48, 20.21), b4 = 16.06 (6.269, 25.85)

a5 = 7.291 (0.02433, 14.56), b5 = 2.691 (-2.965, 8.347)

a6 = -9.384 (-26.23, 7.463), b6 = 9.9 (-13.09, 32.89)

a7 = 4.912 (3.282, 6.543), b7 = 0.1243 (-15.71, 15.96)

a8 = -1.323 (-2.55, -0.09531), b8 = 1.063 (-2.243, 4.369)

w = 0.04519 (0.03991, 0.05047).

Below is the function for the Sum of Sine fitting model:

f(x) = a1*sin(b1*x+c1) + a2*sin(b2*x+c2) + a3*sin(b3*x+c3) +

a4*sin(b4*x+c4) + a5*sin(b5*x+c5) + a6*sin(b6*x+c6) +

a7*sin(b7*x+c7) + a8*sin(b8*x+c8)

where x is normalized by mean 59.51 and std 41.55

Coefficients (with 95% confidence bounds):

a1 = 133.5 (-2.162e+05, 2.164e+05), b1 = 1.387 (-607.2, 610), c1 = -1.971 (-658.7, 654.8)

a2 = 409.4 (-5.372e+07, 5.372e+07), b2 = 2.657 (-8237, 8242), c2 = 3.356 (-4486, 4492)

a3 = 19.2 (-59.64, 98.04), b3 = 6.897 (1.429, 12.36), c3 = -1.994 (-5.398, 1.41)

a4 = 485.3 (-5.35e+07, 5.35e+07), b4 = 2.517 (-8955, 8960), c4 = 0.293 (-5130, 5131)

a5 = 4.653 (-1.774, 11.08), b5 = 14.01 (11.26, 16.76), c5 = 1.591 (0.366, 2.817)

a6 = 16.74 (15.11, 18.37), b6 = 11.09 (9.357, 12.81), c6 = 2.519 (2.016, 3.021)

a7 = 1.673 (0.4056, 2.941), b7 = 16.45 (14.44, 18.46), c7 = 5.584 (3.828, 7.341)

a8 = 4.116 (2.945, 5.288), b8 = 21.19 (20.83, 21.55), c8 = 2.771 (2.472, 3.071)

Based on the smoothing principle, there is no such function generated for curve fitting. I plot all three fitting curves in one figure to visually examine and compare the fitted curve differences.

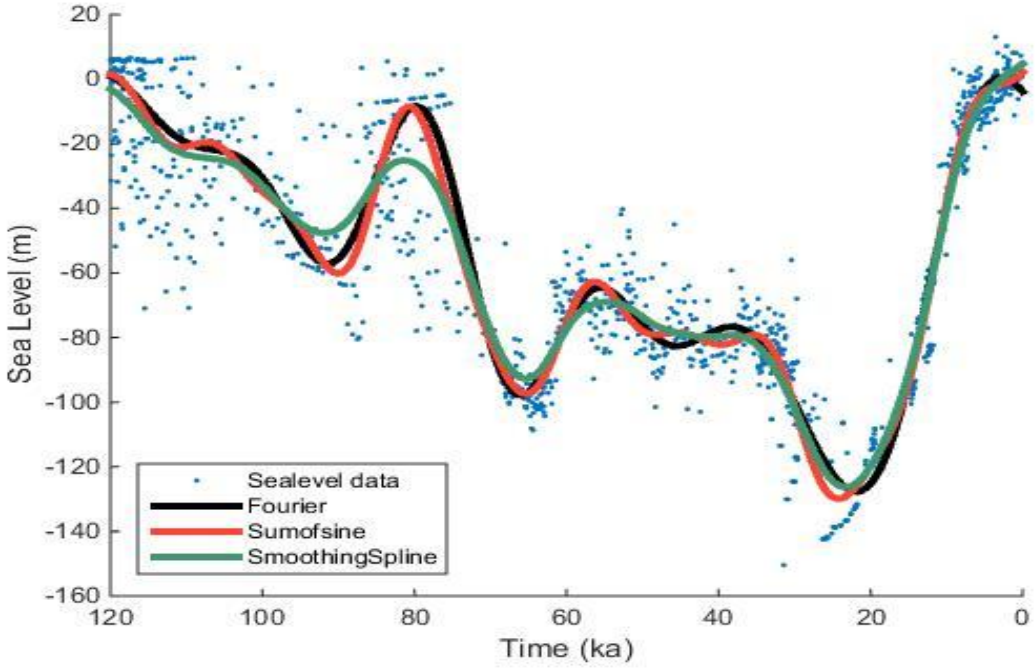

Figure 4.1.2 Comparison of three fit models. The black line is a Fourier series curve, red line is a sum of Sine fitting, and the green line is a Smooth Spline fitting curve.

Table 4.1.1 Goodness of fit results

	Fourier	Sum of Sine	Smooth Spline
SSE	1.6554e+05	1.6314e+05	2.1885e+05
Rsqaure	0.9152	0.9163	0.8879
Dfe	1226	1220	1.2254e+03
Adjrsquare	0.9141	0.9147	0.8863
RMSE	11.6201	11.5733	13.3640
Coef	0.9383	0.9404	0.9424

The table 4.1.1 above shows the goodness-of-fit statistics. For the sum of squares due to error (SSE) a value close to 0 means the model has less random error

possibility and may be more useful in prediction. R-square is defined as the ratio of the sum of squares of the regression (SSR) and the total sum of squares (SST). The R-square close to 1 indicates a greater proportion of observations is described by the model. When increasing the number of fitted variance, R-square will increase as well, so it is better to check the adjusted R-square. Here the sum of sine still has a higher adjusted R-square than the other two models. Another parameter is MSE, the residual mean square of error, $MSE = RMSE^2$. An MSE value close to 0 indicates a better prediction.

Based on two significance tests results, both the Sum of Sine and Smoothing Spline draw great fit curves for global sea level data. From the two predicted sea level curves (Figure 4.1.2), I can say the smoothing curve has an upward trend from 120ka to 140ka; inversely the other one presents a descending trend before 120ka. Also the smoothing curve has a larger slope from current time to the future, which is about 0.24m/kyr, than the sum of sine's slope at 0.20m/kyr.

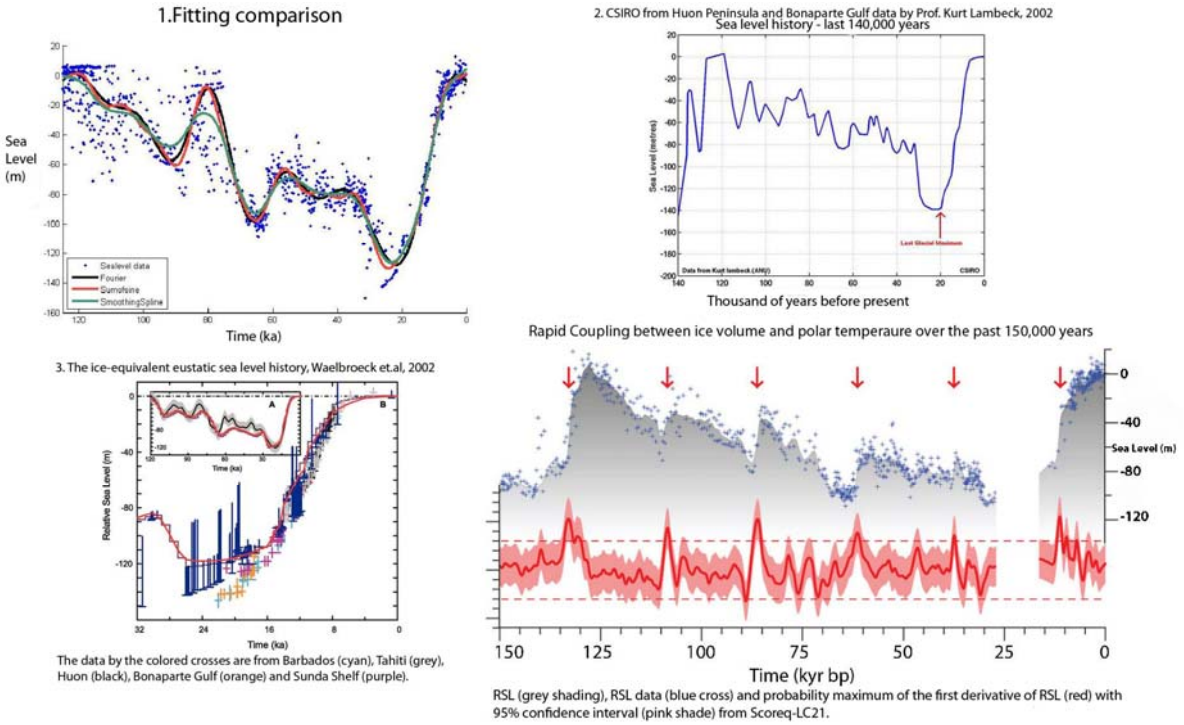

Figure 4.1.3 Comparison of selected sea level curves.

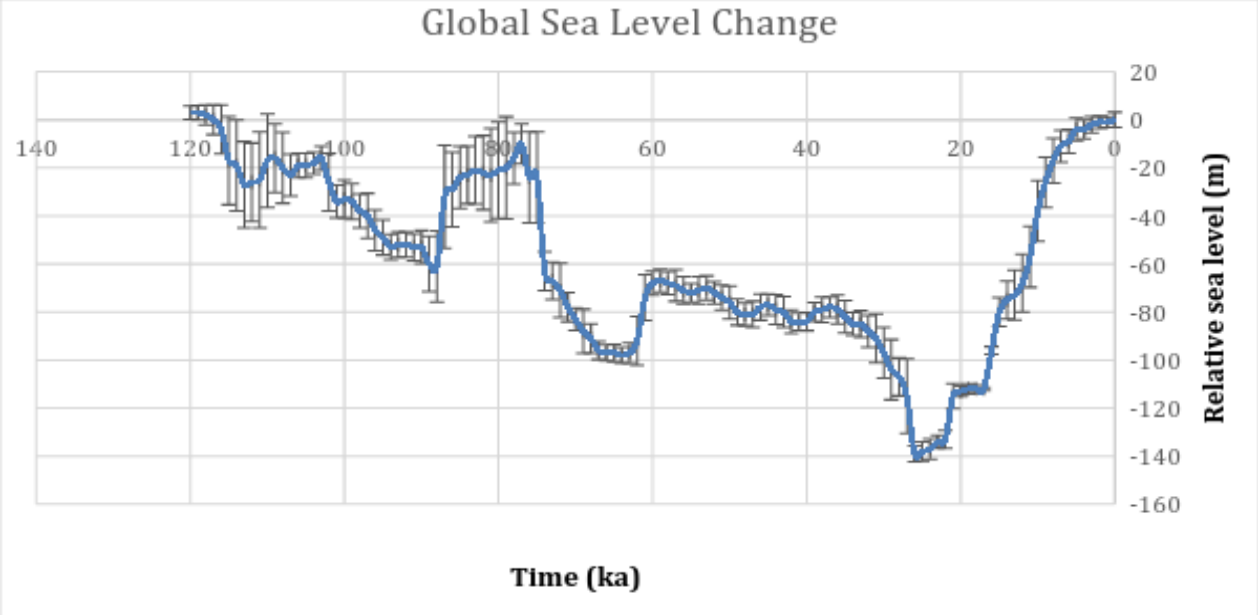

Figure 4.1.4 Sea level change in the past 120,000 years (result from median tendency)

All three Matlab interpolation methods have similar and good predicted results. However they all eliminate some outlier sea level values. Based on the data points and the outliers, I choose to use median values to predict sea levels at every thousand-year interval. The time window is set to 4 thousand years based on some missing values in the whole time span. Figure 4.1.4 shows the result from median of sea level databases at each thousand-year interval and I round them to integers for elevation calculation.

4.2. Trend analysis for each sea level site data

4.2.1. Simple Linear regression

A linear regression model is an effective way to test whether a trend exists in time series data, and it does not require uniformly distributed data. For each site dataset, it is randomly distributed, so I use linear regression to detect if a certain trend exists. However, some datasets may not be suitable for linear regression. Hence, a Pearson-correlation test should be employed before regression. The results of the correlation coefficient for Red Sea, Bermuda, Grand Cayman, and Oahu datasets are very small numbers.

Table 4.2.1.1 Correlation results of *in situ* data

	Barbados	California	Cayucos	Florida Keys	Huon Peninsula	Oregon	Tahiti	West Australia
Pearson Correlation	.801	.909	-.989	.732	.765	-1.000	-.811	.761

Correlation is significant at the 0.01 level

To generate correlation values, I did only 8 linear regressions. The test results are shown below:

Table 4.2.1.2 Linear regression test summary

Site	Barbados	California	Cayucos	Florida Keys	Huon Peninsula	Oregon	Tahiti	West Australia
R-Square	.642	.826	.979	.536	.585	1.000	.658	.579
Coefficient	17.670	16.722	-20.342	6.970	10.617	-83.658	-13.804	6.534
ANOVA F	312.245	279.624	413.777	48.587	112.712	6998.634	190.557	42.692
Sig.	0.000	0.000	0.000	0.000	0.000	0.008	0.000	0.000

ANOVA F ratio is the ratio of two mean square values, $F = \frac{MS_{regression}}{MS_{residual}}$. If the null hypothesis is true, the F-ratio value should be close to 1. The testing R-square and F-ratio values are very big in all cases, and P-values are all smaller than 0.05. At the α=0.05 level of significance, I can reject the null hypothesis that time is not a useful predictor of sea level. Thus the result of the linear regression shows that there is some trend in sea level change at each site during its own study period. However for

some datasets such as Barbados, Huon Peninsula and Tahiti, the time span is longer than 20,000 years and this may lead to less accurate results in the linear regression.

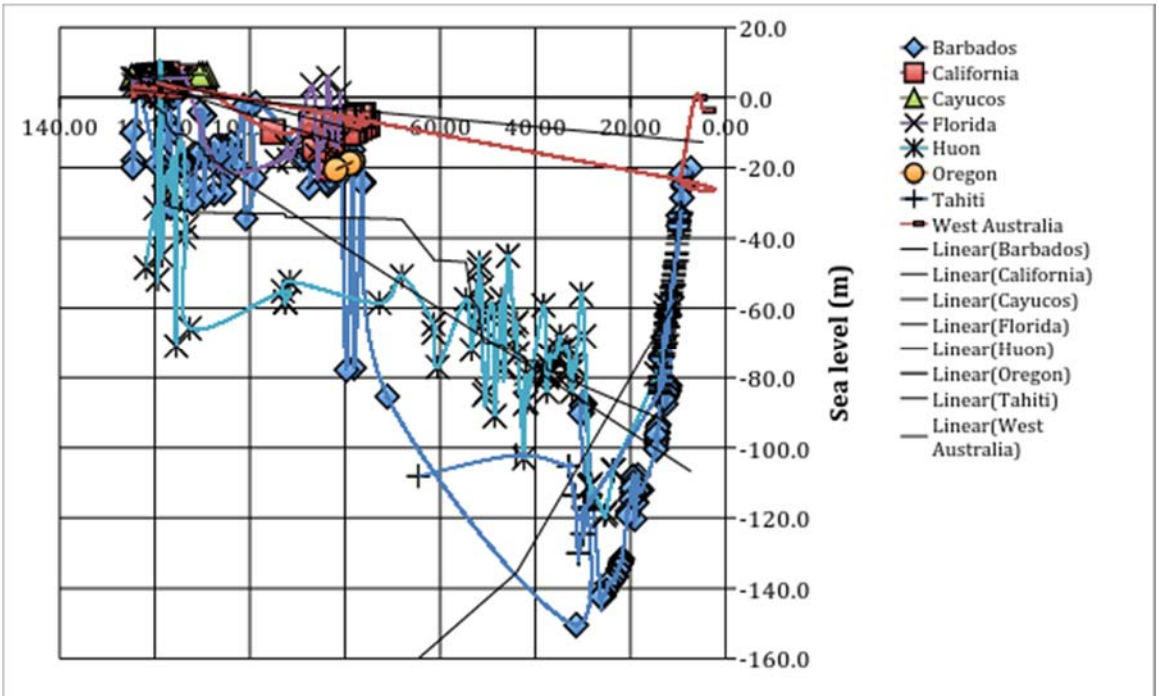

Figure 4.2.1.1 Simple linear regressions for each sample site

4.2.2. Mann-Kendall trend test

The S, t, z-value, and p-value are calculated for each sea level data using the modified Mann-Kendall trend test. According to the Matlab TFPW Mann-Kendall test, the varS value, the t value, the z-value, and the p value are shown as Table 4.2.2.1. For Bermuda and Grand Cayman, the p value is equal to 0.5 which means there is no trend exists. The P value is > 0.5, indicating there is a positive trend exists; the P value is <0.5, indicating there is a negative trend. The sea level change data in other

10 sample sites has a negative trend that means the sea level had a monotonic downward trend over each time span.

Table 4.2.2.1 Modified Mann-Kendall Trend Test Results

	VarS	t	z	p
Red Sea	34399950	-0.00023	-0.00904	0.4964
Barbados	610866	0.010974	0.216229	0.4144
California	8.6666	0.022951	0.261362	0.3969
Cayucos	165	-0.18182	-0.7785	0.2181
Huon	62361	0.021379	0.284316	0.3881
Oahu	8514	-0.01278	-0.11921	0.4526
Oregon	3.66667	-0.6667	-1.04445	0.1481
Tahiti	116150	-0.0198	-0.2934	0.3846
West	4165	0.0038	0.031	0.4876
Florida	9775	0.011628	0.1113	0.4557

4.3. Global land distribution curve and total area change from ETOPO1

Based on the predicted sea level change data and its extreme values during the past 120,000 years, I created 17 global land and sea maps. In these maps the red color means during that time land now submerged was exposed.

World Elevation Map 0ka

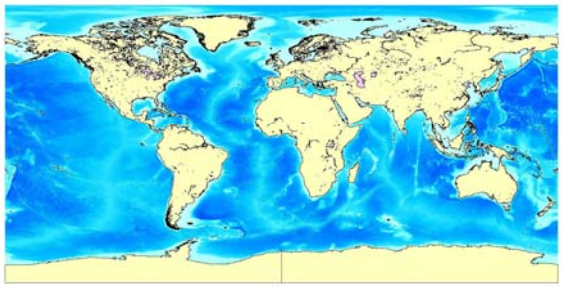

World Elevation Map 26ka

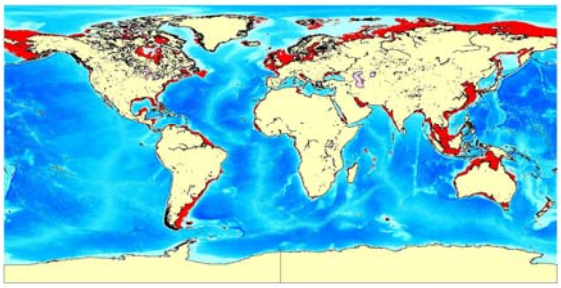

World Elevation Map 59ka

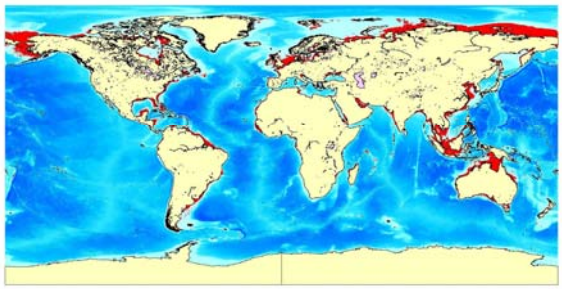

World Elevation Map 64ka

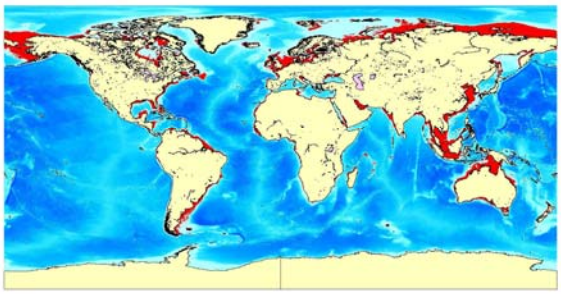

World Elevation Map 77ka

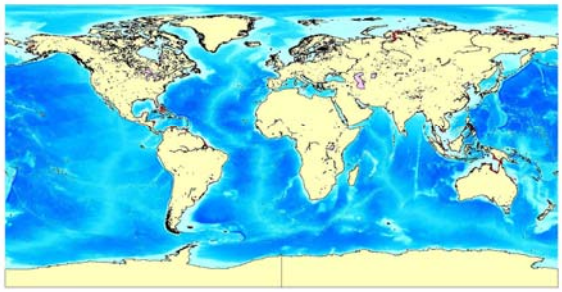

World Elevation Map 88ka

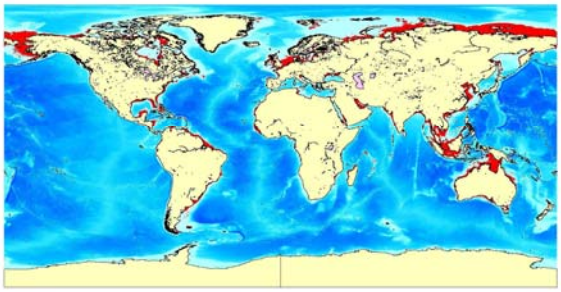

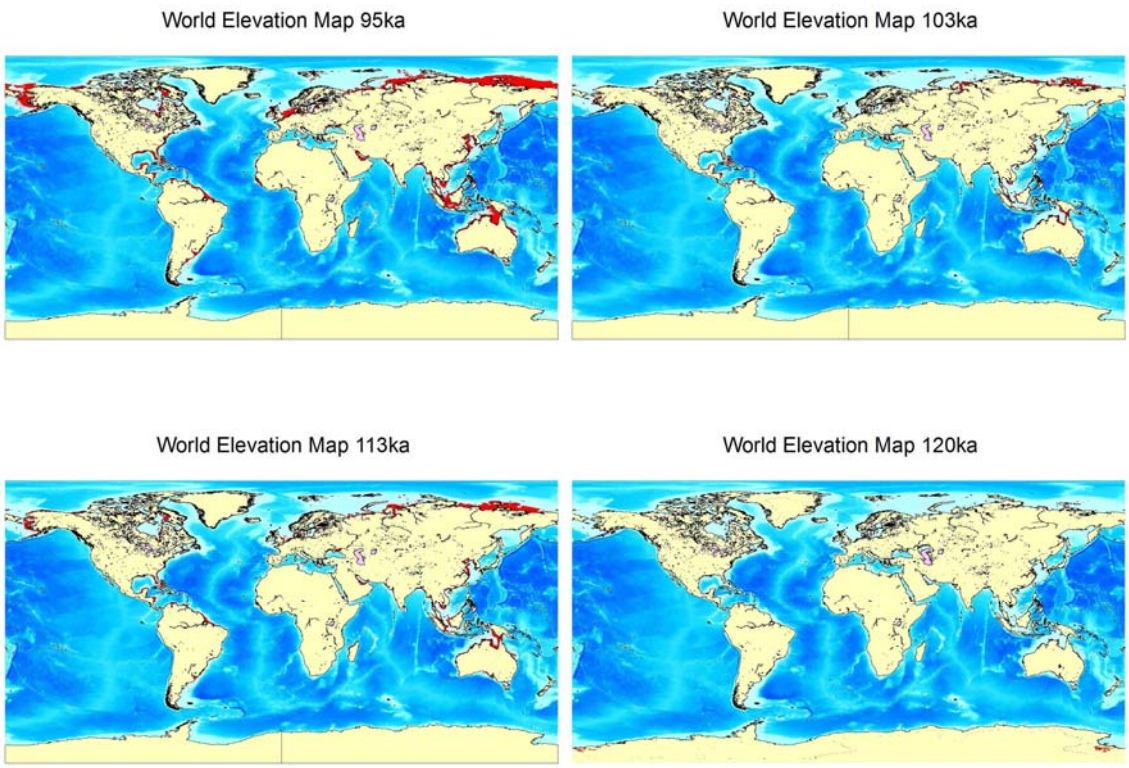

Figure 4.3.1 World elevation maps from predicted sea level curve at 10 extreme values

Clearly, when sea level was lower, more of aquaterra's land was exposed: In Europe, parts of the North Sea, Baltic Sea, Gulf of Bothnia, and Mediterranean Sea and Black Sea shrank; the far northern part of Russia (most of this area was covered by ice sheets and unsuitable for habitation); south and east part of Asia especially Malaysia, Philippines and Indonesian islands were connected to the mainland; the Persian Gulf disappeared and the northern part of the Red Sea as well; Australia was connected with Papua New Guinea and Indonesia when the sea level was only about 20 meters lower; most of the southern coastal area of North America and South America; and eastern Siberia and the United States' state of Alaska was connected by

what is often called a land bridge but was actually a vast coastal plain during the late Pleistocene ice ages.

4.3.1. Inland water bodies

Inland seas would not have fluctuated with world ocean levels, the only one that would have changed in sync with the world ocean is the Black Sea, which is connected when world ocean levels are high and inland when world ocean levels are low. My focus is on the world ocean so I kept the levels of inland seas constant by adjusting inland water bodies' surface change without eustatic rise and fall. The GSHHS lake contours and ETOPO1 data readily identify large inland water areas such as the Caspian Sea, Great Lakes, and Lake Eyre Basin, which is inland water body or have part inside a basin which is lower than current sea level. When calculating land area change through time, I decided not to count the area of all inland water bodies except the Black Sea from total land area change. When there is a slope exists in water body, the true surface area of a landscape is greater than its projected surface area. For every meter change in elevation, I calculate the area between each set of contour lines that are 1-meter apart with different latitude and longitude. The resolution of the DEM model is 1 arc-minute, which is equal to one sixtieth of a degree when using grid cell resolution, or about 1.8 km. All inland water bodies data were extracted from GSHHS boundaries in Matlab.

The Caspian Sea is the largest enclosed inland water body on Earth. It has a surface area of 371,000 $km^2$and a volume of 78,700 km^3. The lowest point in Southern Caspian has a maximum depth reaching over 1000 m below the current mean sea level.

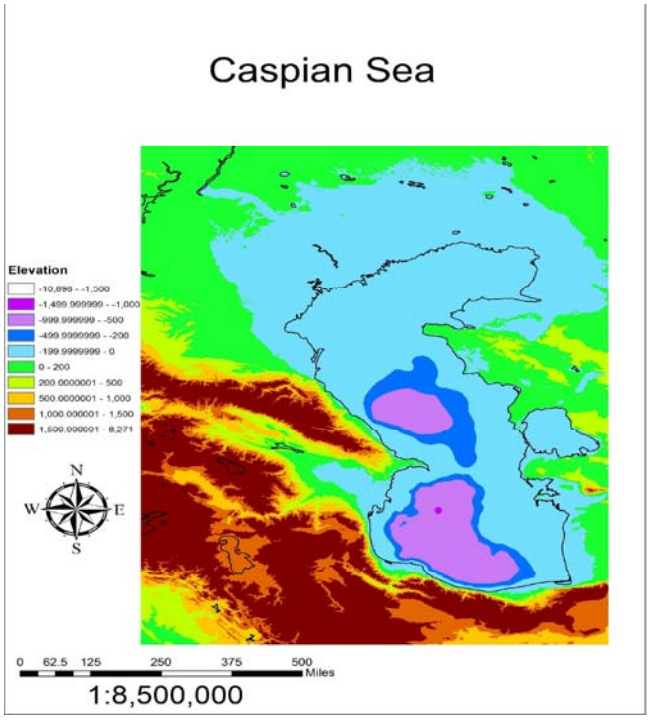

Figure 4.3.1.1 Caspian Sea Bathymetry map

The Great Lakes are a series of interconnected freshwater lakes located in northeastern North America, on the Canada-United States border. Due to their sea-like characteristics: rolling waves, sustained winds, strong currents, great depths, and distant horizons, the five Great Lakes have also long been referred to as inland seas. However Lake Ontario flows to the North Atlantic Ocean through the St.

Lawrence River. They would have been covered by Laurentide Ice Sheet whenever world ocean levels were low.

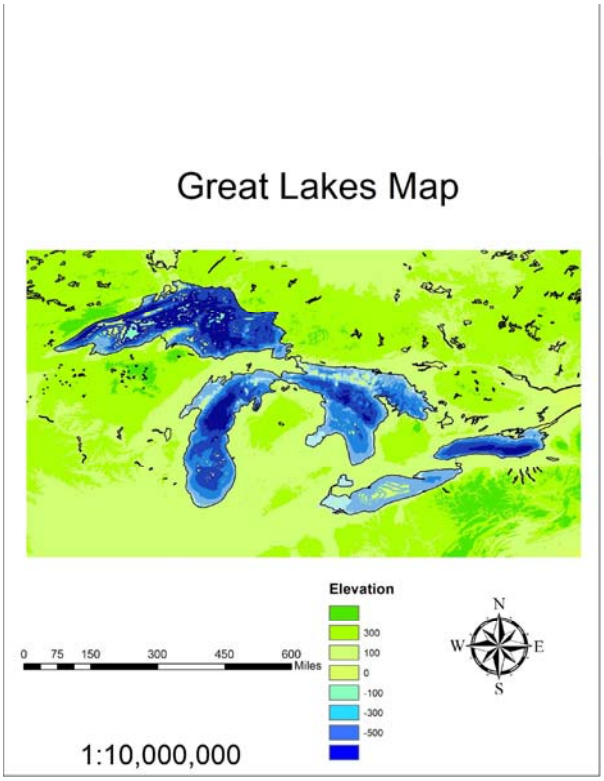

Figure 4.3.1.2 Great Lakes Bathymetry map

The Lake Eyre Basin is the largest endorheic basin, an internal drainage basin that does not flow to the Earth's oceans or rivers, in Australia and amongst the largest in the world, covering about 1,200,000 square kilometers (463,323 sq. mi). The lowest parts of Lake Eyre, a great salt lake in south central Australia, lie about 15.2 m below world ocean level.

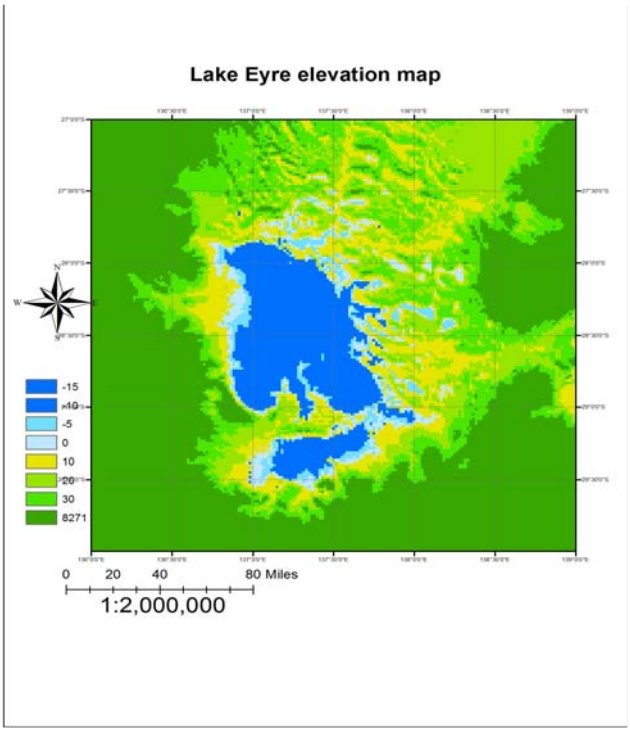

Figure 4.3.1.3 Lake Eyre Basin map

The elevation data are extracted from ETOPO1 Ice Surface data through Matlab. The latitude and longitude range for Caspian Sea, Great Lakes, and Lake Eyre Basin respectively are $35\ ° \ to\ 50°, 40° \ to\ 50°, -30° \ to\ -27°, and\ 43° \ to\ 56°, -93° \ to\ -75°, 136° \ to\ 139°$. The returned DEM files are 900*780, 600*1080, and 180*180 matrices in which each point is an elevation. The area of each cell decreases with increasing latitude. For instance, at north or south 27°, the area of each 1 degree lat/lon cell is 3.05 km^2, while at 50° it is 2.215 km^2.

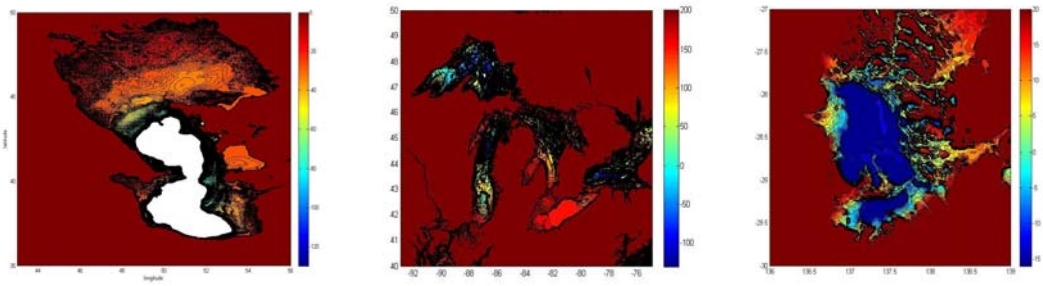

Figure 4.3.1.4 Contour maps of the Caspian Sea, Great Lakes, and Lake Eyre

There are more than 6000 inland lakes and seas around the world; I remove all these areas from my global calculation. The total surface area of these lakes is 2,640,205.197km^2. The global land area change has, of course, an inverse trend with sea level change (Figure 4.3.1.5).

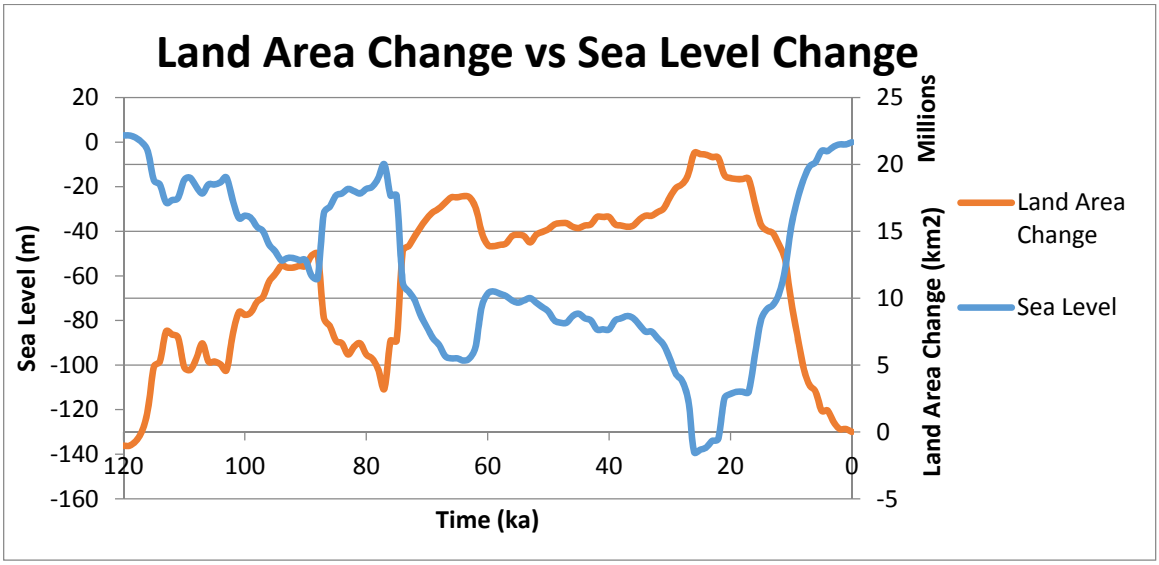

Figure 4.3.1.5 Global Land Area change over the past 120,000 years (with inland waterbodies held constant at current levels).

4.3.2. Global Land Area Chang by Latitudinal and Longitudinal Zone

Based on ETOPO1 data, the land areas are predominantly distributed in the Northern Hemisphere relative to the Southern Hemisphere which is 68% to 32% in total landmasses. As Earth evolved through time the distribution of terrestrial lands changed dramatically. Below is a current land distribution by latitude (based on the ellipsoid model with the Earth as a sphere with a radius of 6378 km):

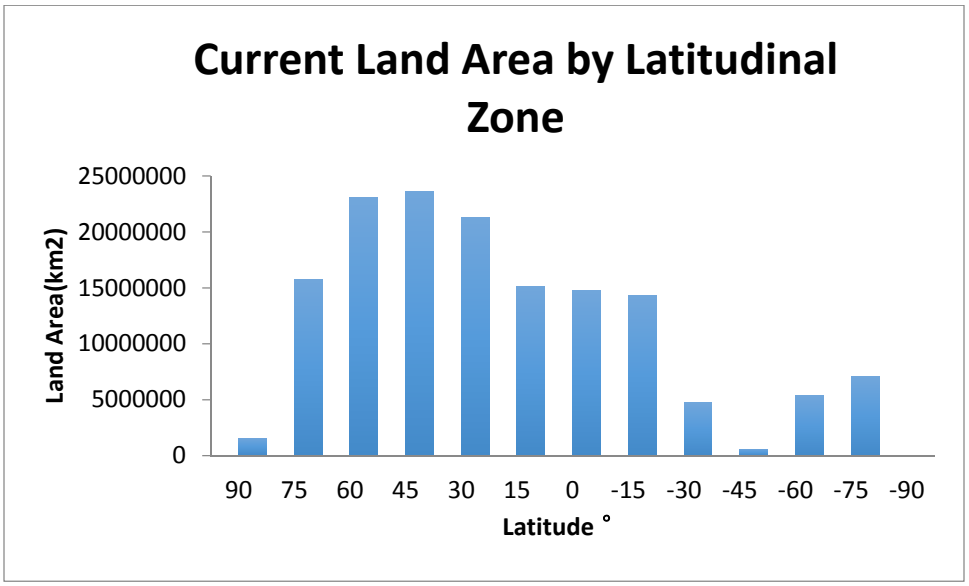

Figure 4.3.2.1 The distribution of land areas in 15-degree increments.

From this graph, most land is between 45 ° S and 75 ° N (Figure 4.3.2.1). From 75° S to the South Pole, most land is covered by ice in Antarctica. Normally tropical areas can reach as far as 23.5° N and 23.5° S, so I decided to calculate land area change in these latitude areas: 66.5° S to 23.5° S, 23.5 ° S to 0 °, 0 ° to 23.5 ° N, 23.5 ° N to 66.5 °

N, labeled as Zone 1 to Zone 4. Total land area changes through the past 120,000 years are shown as below:

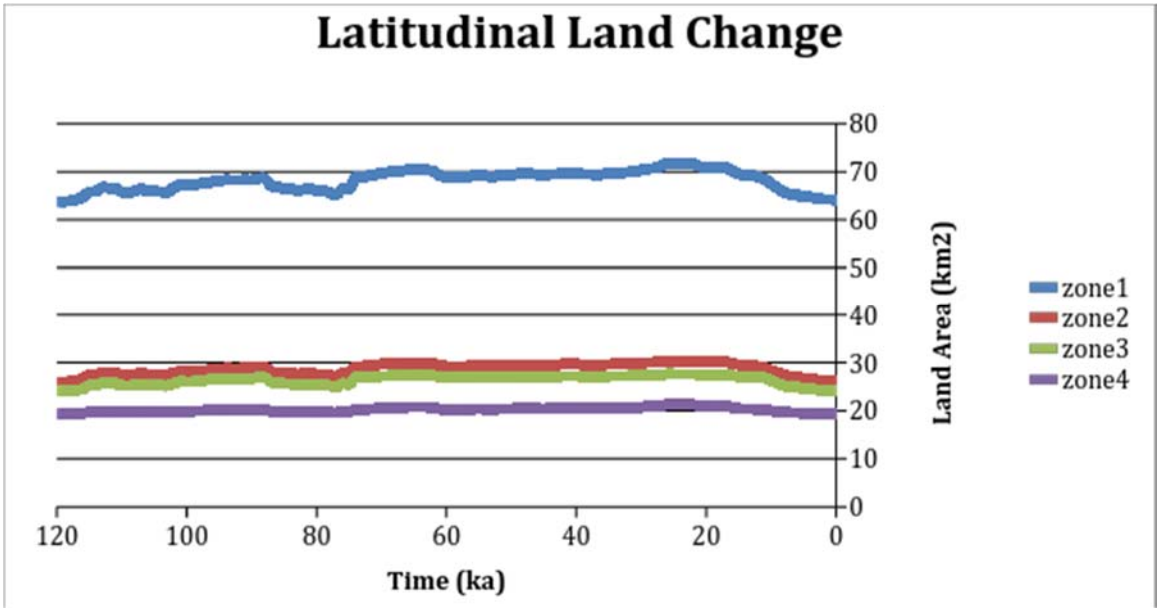

Figure 4.3.2.2 Global land area change by latitudinal zone

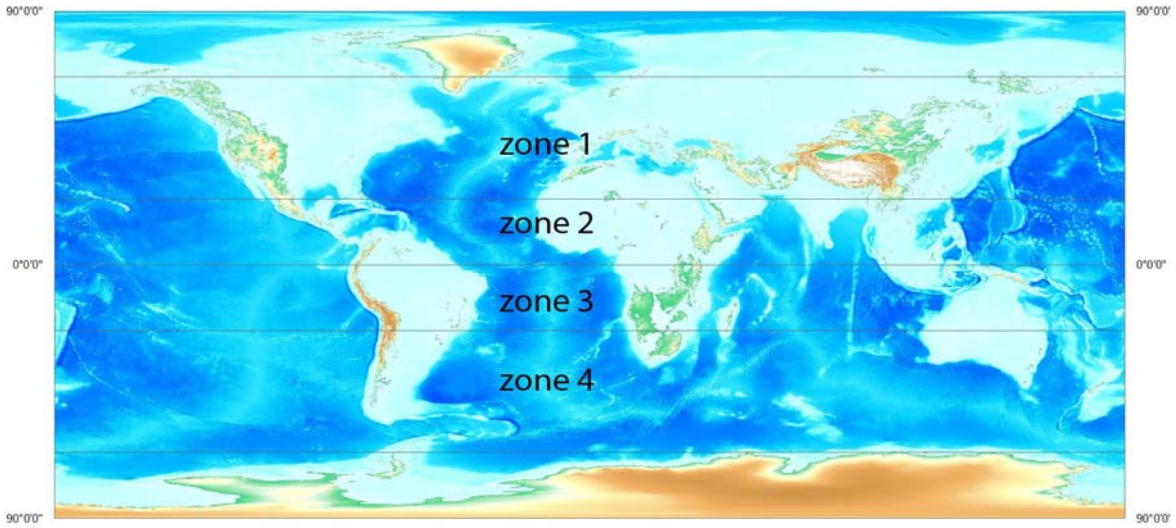

Figure 4.3.2.3 Latitudinal zone map

The land distribution has similar change trend in all zones, however the area between 23.5 ° N and 66.5 ° N (North Temperate Zone) has the biggest change in total land area. Also land area between 0° to 66.5° N is much larger than those between 0° to 66.5° S.

Then I calculated the land distribution change for longitudinal zones of every 30 degrees.

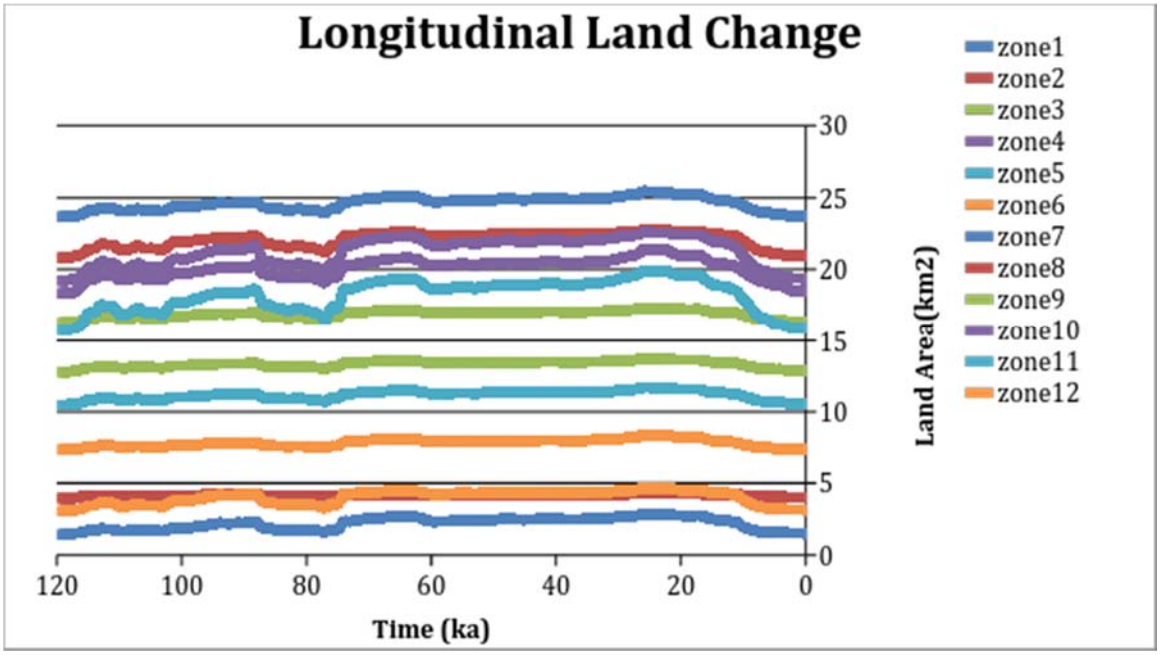

Figure 4.3.2.4 The longitudinal distribution of land areas in every 30° zone

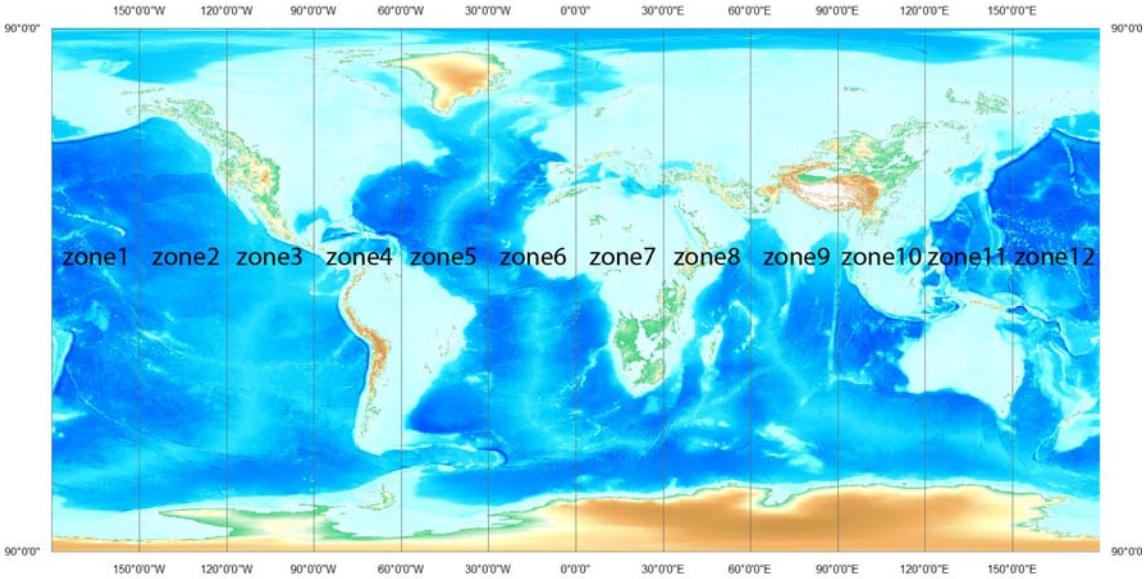

Figure 4.3.2.5 Longitudinal zone map

Most land is in the Eastern hemisphere (Figure 4.4.2.4). Similarly, when sea level fell, more land was exposed in the Eastern hemisphere because the continental shelf slope is less steep or shallower than land in Western hemisphere.

5. Discussion

This study focuses on how the global sea level changed and how it affected terrestrial and submerged land (aquaterra) distributions. The predicted late Pleistocene and Holocene sea level change derived from 12 *in situ* data supports other sea level change findings (ref.) and has similar trend such as reached the lowest level during the LGM and rose to above current sea level around 120,000 years ago. The global mean sea level values are built without eustatic rise and fall. However my lowest level is 139 meters below current sea level at 26,000 years ago compared to others sea level records (Table 2.1.1). Trend analysis results show the local sea level did rise or fall in specific time windows.

Nonlinear regression models (Fourier series, sum of sine and smoothing spline) and central tendency measurement are used to fit the global sea level change from *in situ* data. From the curve, clearly recent data are more concentrated due to higher accuracy techniques and more reliable data samples. The older observations are more scattered, ranging from 61 meters below to 3 meters above current sea level at 88ka to 120ka. Thus, predicted value is more reliable during the last 60,000 years than those before. Although three regression models have great correlation with the original databases, some outliers are eliminated due to regression properties. The median values of 12 data sets are selected to demonstrate global mean sea level at every thousand-year interval considering the past trend of the curve. When creating

sea level change maps, due to the resolution of DEM data which is no better than 1 meter, all predicted sea level values are rounded to integers. An animation of sea level change is made using the predicted data (See Appendix).

Changes in sea level can be directly linked to atmospheric and oceanic processes. A simple linear trend analysis for a single sea level data set shows Tahiti sea level was rising from about 65,000 years ago, while others had generally declining with some periodic fluctuations except for the Red Sea, Bermuda, Grand Cayman, and Oahu datasets (Figure 4.2.1.1). However a small t value (0.0159) and big p value (0.3960) in TFPW MK test shows there is no monotonic upward (downward) trend in global sea level change during the last 120,000 years.

In order to get the terrestrial land change caused by global sea level change, I remove all inland water bodies from global land area calculation and assume they are constant. Landmass distribution changes are classified by latitude and longitude zones. Latitude zones are defined by three main climate zones—tropical, temperate, and polar. From distribution of land areas results (Figure 4.4.2.2 and Figure 4.4.2.4), I can say the land is predominantly distributed in the Northern hemisphere and Eastern hemisphere. The land between 66.5° N and 23.5° N (north temperate zone) and 23.5° S to 23.5° N (tropical zone) experienced relatively greater area change when sea level was lower.

When using latitude zones to calculate the land distribution, the land between the equator and 66.5° N takes up more than 58.58% of the total land area. While using longitude lines to analyze the distribution change, the land area is predominantly distributed in the Eastern Hemisphere at 64.48% relative to the Western Hemisphere at 35.52% in total global land. The higher percentages mean more land is available for human development and for migration among islands and mainlands. Below is a table showing latitudinal area changes (aquaterra area in latitudinal zones percentage):

Table 5.1 Aquaterra latitudinal changes by climate zones

	North temperate zone	Northern tropic	Southern tropic	South temperate zone
Occupy percentage	36.77%	19.88%	15.93%	9.03%
Change percentage	12.61%	16.72%	14.41%	10.21%

The total land area for aquaterra is about 21,867,064.38 km^2, which is slightly different from the 24,464,906 km^2 Dobson's calculation (Dobson, 2014). This is because my sea level is from -139 m to +3 m from fitting curve, compared to his which as -125 m to +5 m. It takes up to 12.5% of the global land area at its lowest sea level.

Although sea level fluctuated dramatically during the last 120,000 years, a truly accurate sea level change is hard to get due to lack of data. Since I am doing sea level change at the global scale, the uncertainties such as eustatic changes due to glacial

rebound in coastal areas are not considered. In order to get a more precise land change, inundation models can be used to evaluate land in risk, but that is beyond the scope of my analysis.

6. Conclusion

Much more needs to be known about physical and human processes during the Late Pleistocene and Holocene ages. Most of the world's population is dispersed at lower elevation close to coastlines. There is a crucial need for better understanding of climate change and risks associated with sea level rise in coastal areas. Three regression models and central tendency are used to predict global sea level change from 12 *in situ* databases during the last 120,000 years. The median value works the best according to the significance test and correlation coefficient. The result shows the sea level reached its lowest point at 139 meters lower at 24,000 years ago and was 3 meters higher than current sea level at 120,000 years ago. Based on high resolution digital elevation model data and my estimated sea level data, my animation, consisting of 17 global sea level change maps, reveals the change of terrestrial and submerged land over time. The exposed portions of quaterra area are shown as a red color in the animation.. When sea level was lower, most continental shelf areas in Europe, Southeast Asia, Australia, the southern part of North America, and South America were exposed.

Short-term sea level change has monotonic trend such as sea level at Cayucos and Oregon is rising during 125 to 109ka and 82 to 78ka. Clearly, the global sea level change is periodic and can be linked with climate change.

Most of the Earth's land is distributed in the Northern hemisphere and Eastern hemispheres after adjusting the inland water bodies' areas (figure 4.4.2.2 and figure 4.4.2.4). Aquaterra is not normally distributed around the world and more land was exposed in Northern hemisphere than Southern hemisphere when sea level was lower. With the new detailed maps, given an archaeological site, one can tell approximately if it was exposed at a certain time. Thus, underwater ruins can be tested for depth and time according to the aquaterra change map.

Further research such as add detailed paleo climatic data or simulation models with the global topo map, or focus on smaller area's sea level change (relative sea level change) and land distribution change, historical human movements can be better understood.

7. References

1. Intergovernmental Panel on Climate Change (IPCC) Fourth Assessment Report: Climate Change 2007

2. The Southern Route "Out of Africa": Evidence for an Early Expansion of Modern Humans into Arabia

3. United Nations Population Division (1997) World Urbanization Prospects: The 1996 Revision (United Nations, New York)

4. Bailey, G.N., and Flemming, N.C., 2008. Archaeology of the Continental Shelf: Marine Resources, Submerged Landscapes and Underwater Archaeology. *Quaternary Science Reviews* **27**, 2153-2165.

5. Bard, E., B. Hamelin, R. G. Fairbanks, A. Zindler, 1990. Calibration of the 14C timescale over the past 30,000 years using mass spectrometric U-Th ages from Barbados corals. *Nature* **345**, 405-410.

6. Bard, E., Hamelin, B., Fairbanks, R.G., 1990. U/Th ages obtained by mass spectrometry in corals from Barbados: Sea level during the last 130,000 years. *Nature* **364**, 456-458.

7.Bard, E, B. Hamelin, M. Arnold, L. Montaggioni, G. Cabioch, G. Faure, and F. Rougerie, 1996. Deglacial sea-level record from Tahiti corals and the timing of global meltwater discharge. *Nature* **382**, 241-244.

8.Calvin, W. H. 1990. *The Ascend of Mind: Ice Age Climates and the Evolution of Intelligence.* New York: Bantam Dell Publishing Company.

9.Carter, R.M.; Johnson, D.P. 1986 Sea-level controls on the post-glacial development of the Great Barrier Reef, Queensland. Marine Geology, v.71:137-164.

10.Cavalli-Sforza, L. L., P. Menozzi, and A. Piazza. 1993. Demic Expansions and Human Evolution. *Science* **259** (5095): 639646.

11.Chappell, J., and N. J. Shackleton. 1986. Oxygen Isotopes and Sea Level. *Nature* **324**, 137-140.

12.Chappell, J., and H. Polach, 1991. Post-glacial sea-level rise from a coral record at Huon Peninsula, Papua New Guinea. *Nature* **349**, 147-149.

13.Chappell, J., A. Omura, T. East, M. McCulloch, J. Pandolfi, Toko Ota, and Brad Pillans. 1996. Reconciliation of late Quaternary sea levels derived from coral terraces at Huon Peninsula with deep sea oxygen isotope records. *Earth and Planetary Science Letters* **141**, 227-236.

14.Clark, P.U., and A.C. Mix, 2002. Ice Sheets and Sea Level of the Last Glacial Maximum. *Quaternary Science Reviews* **21**,1-7.

15.Cohen, J. E., and C. Small. (1998). Hypsographic demography: The distribution of the human population by altitude. *Proc. Nat. Acad. Sci. USA*, **95**, 14009–14014.

16.Colonna, M. J., Casanova, J., Dullo, W. C., and Camoin, G. 1996. Sea-level changes and δ18O record for the past 34,000 yr from Mayotte reef, Indian Ocean. *Quaternary Research* **46**, 335–339.

17.Coyne, M. K., Jones, B. & Ford, D. 2007. Highstands during Marine Isotope Stage 5: evidence from the Ironshore Formation of Grand Cayman, British West Indies. *Quaternary Sci Rev* **26**, 536-559.

18.Cuffey, K.M., and S.J. Marshall, 2000. Substantial contribution to sea-level rise during the last interglacial from the Greenland ice sheet. *Nature* **404**, 591-594.

19.Cutler, K. B. et al. 2003. Rapid sea-level fall and deep-ocean temperature change since the last interglacial period. *Earth Planet Sc Lett* **206**, 253-271.

20.Dobson, Jerome E. 2014. Aquaterra *Incognita*: Lost Land beneath the Sea. *Geographical Review*, **104**:123-138.

21.Dodge, R.E., R. G. Fairbanks, L. K. Benninger and Maurrasse, F. 1983. Pleistocene sea levels from raised coral reefs of Haiti. *Science*, **219**, 1423-1425.

22.Eakins, B.W. and G.F. Sharman. Hypsographic Curve of Earth's Surface from ETOPO1, NOAA National Geophysical Data Center, Boulder, CO, 2012

23.Esat M. T. et al. 1999. Rapid Fluctuations in Sea Level Recorded at Huon Peninsula During the Penultimate Deglaciation. *Science* **283**, 197.

24.Esat, T. M., McCulloch, M. T., Chappell, J., Pillans, B. & Omura, A. 1999. Rapid fluctuations in sea level recorded at Huon Peninsula during the Penultimate Deglaciation. *Science* **283**, 197–201.

25.Fairbanks, R.G., 1989. A 17,000-year glacio-eustatic sea level record: influence of glacial melting dates on the Younger Dryas event and deep ocean circulation. *Nature* **342**, 637-642.

26.Fairbanks, R. G. et al. 2005. Radiocarbon calibration curve spanning 0 to 50,000 years BP based on paired Th-230/U-234/U-238 and C-14 dates on pristine corals. *Quaternary Sci Rev* **24**, 1781-1796.

27.Ferland, M. A., Roy, P. S. and Murray-Wallace, C. V. 1995) Glacial lowstand deposits on the outer continental shelf of southeastern Australia. *Quaternary Research* **44**, 294-299.

28.Fleming, K., Johnston, P., Zwartz, D., Yokoyama, Y., Lambeck, K., and Chappell, J. 1998. Refining the eustatic sea-level curve since the Last Glacial Maximum using far- and intermediate-field sites. *Earth Planet. Sci. Lett.* **163**, pp. 327–342.

29.Gallup, C.D., Edwards, R.L., Johnson, R.G., 1994. The timing of high sea levels over the past 200,000 years. *Science* **263**, 796-800.

30.Gallup, C. D., Cheng, H., Taylor, F. W. & Edwards, R. L. 2002. Direct determination of the timing of sea level change during termination II. *Science* **295**, 310-313.

31.Gamble, Clive. Settling the Earth: The Archaeology of Deep Human History. Cambridge University Press. 2013.

32.Gehrels, W.R., Milne, G.A., Kirby, J.R., Patterson, R.T., and Belknap, D.F., 2004. Late Holocene sea-level changes and isostatic crustal movements in Atlantic Canada. *Quaternary International* **120**, 79-89.

33.Geyh, M.A., H. Streif, and H.-R. Kudrass. 1979. Sea-level changes during the late Pleistocene and Holocene in the Strait of Malacca. *Nature* **278**,441-443.

34.Gilbert, R. O. 1987. Statistical Methods for Environmental Pollution Monitoring. Van Nostrand Reinhold Co., New York, 320 p.

35.Grant, K.M., E.J. Rohling, M. Bar-Matthews, A. Ayalon, M. Medina-Elizalde, C. Bronk Ramsey, C. Satow, A.P. Roberts. 2012. Rapid coupling between ice volume and polar temperature over the past 150,000 years. *Nature* **491**, 744-747.

36.Gretton, E.J. 2002. Palaeoceanographic Changes Offshore New Caledonia for the Past 140,000 Years. Department of Earth and Planetary Sciences. Australian National University, Canberra (2002), p. 104.

37.Hamed, Khaled H.; Ramachandra Rao, A. 1998. A modified Mann-Kendall trend test for autocorrelated data. *Journal of Hydrology*, V**204**, Issue 1, p. 182-196.

38.Hanebuth, T., Stattegger, K., and Grootes, P.M., 2000. Rapid Flooding of the Sunda Shelf: A Late-Glacial Sea-Level Record. *Science* **288**, 1033-1035.

39.He,L.J., Zhang, A.B., Weesc, D., Zhu, C.D., Jiang, C.J., and Qiao, Z.G. 2010. Late Pleistocene population expansion of Scylla paramamosain along the coast of China: A population dynamic response to the Last Interglacial sea level highstand. *Journal of Experimental Marine Biology and Ecology* **385**, 20-28.

40.Jacobs, D.K., and Sahaguan. L.L. 1993. Climate-induced Fluctuations in Sea Level during Non-glacial times. *Nature* **361**, 710-712.

41.Kendall, M.G. 1975. Rank correlation methods. Griffin: London.

42.Kirwan, M.L., and Megonigal, J. P., 2013. Tidal wetland stability in the face of human impacts and sea-level rise. *Nature* **504**, 53-60.

43.Lambeck, K., and J. Chappell. 2001. Sea Level Change through the Last Glacial Cycle. *Science* **292**: 679-685.

44.Lambeck, K., Tezer M. Esat, and Emma-Kate Potter. 2002. Links between climate and sea levels for the past three million years. *Nature* **419**, 199-206.

45.Linsley, B.K., 1996, Oxygen isotope evidence of sea level and climatic variations in the Sulu Sea over the past 150,000 years. *Nature* **380**, 234-237.

46.Ludwig, K. R., Muhs, D. R., Simmons, K. R., Halley, R. B. & Shinn, E. A. 1996. Sea-level records at similar to 80 ka from tectonically stable platforms: Florida and Bermuda. *Geology* **24**, 211-214.

47.Mamo, B.L., G. A. Brock and E. J. Gretton. 2013. 'Deep-sea benthic Foraminifera as proxy for palaeoclimatic fluctuations in the New Caledonia Basin, over the last 140,000 years. *Marine Micropaleontology* **104**:1–13.

48.Manderscheid, E.J. and A.R. Rorgers. 1996. Genetic Admixture in the Late Pleistocene. *American Journal of Physical Anthropology* **100**: 1-5.

49.Mann HB. 1945. Nonparametric tests against trend. *Econometrica* **13**: 245–259.

50.Muhs, D. R., Simmons, K. R., Schumann, R. R. & Halley, R. B. 2011. Sea-level history of the past two interglacial periods: new evidence from U-series dating of reef corals from South Florida. *Quaternary Sci Rev* **30**, 570-590.

51.Muhs, D. R., Simmons, K. R. & Steinke, B. 2002. Timing and warmth of the Last Interglacial period: new U-series evidence from Hawaii and Bermuda and a new fossil compilation for North America. *Quaternary Sci Rev* **21**, 1355-1383.

52.Muhs, D. R., Simmons, K. R., Kennedy, G. L. & Rockwell, T. K. 2002. The last interglacial period on the Pacific Coast of North America: Timing and paleoclimate. *Geol Soc Am Bull* **114**, 569-592.

53.Muhs, D.R, et al., 2006. A cool eastern Pacific Ocean at the close of the Last Interglacial complex. *Quaternary Sci Rev* **25**, 235-262.

54.Murray-Wallace, C.V. 2007b: Sea level studies: eustatic sea-level changes since the last glaciation. In Elisa, S.A., editor, Encyclopedia of Quaternary science, Amsterdam: Elsevier, 3034-43.

55.Nakada, M. & Lambeck, K. 1988. The melting history of the Late Pleistocene Antarctic ice sheet. *Nature* **33**, 36–40.

56.Peltier, W., and R. G. Fairbanks. 2006. Global Glacial Ice Volume and Last Glacial Maximum duration from an Extended Barbados Sea Level Record. *Quaternary Science Reviews* **25** (23-24): 3322-3337.

57.Pirazzoli, P.A. 1993. Global sea-level changes and their measurement. *Global and Planetary Change* **8**, 135-148.

58.Siddall,M., E. J. Rohling, A. Almogi-Labin, Ch. Hemleben, D. Meischner, I. Schmelzer and D. A. Smeed. 2003. Sea-level fluctuations during the last glacial cycle. *Nature* **423**: 853-858.

59.Shennan, I. 2007: Ses level studies: overview. In Elias, S.A., editor, Encyclopedia of Quaternary science, Amesterdam: Elsevier, 2967-74.

60.Small, C. and J.E., Cohen. 1999. Continental physiography, climate and the global distribution of human population. *Proceedings of the International Symposium on Digital Earth,* Science Press, Beijing, pp. 965-971.

61.Small. C. and R.J., Nicholls. 2003. A Global Analysis of Human Settlement in Coastal Zones. *Journal of Coastal Research*, **19**:584-599.

62.Snedecor, George W. and Cochran, William G. 1989. *Statistical Methods*. Eighth Edition, Iowa State University Press.

63.Speed, R. C. & Cheng, H. 2004. Evolution of marine terraces and sea level in the last interglacial, Cave Hill, Barbados. *Geol Soc Am Bull* **116**, 219-232.

64.Stein, M. et al. 1993. Tims U-Series Dating and Stable Isotopes of the Last Interglacial Event in Papua-New-Guinea. *Geochim Cosmochim Ac* **57**, 2541-2554.

65.Stirling, C. H ., Esat, T. M., Lambeck, K. & McCulloch, M. T. 1998. Timing and duration of the Last Interglacial: evidence for a restricted interval of widespread coral reef growth. *Earth Planet Sc Lett* **160**, 745-762.

66.Stirling, C. H., Esat, T. M., McCulloch, M. T. & Lambeck, K. 1995. High-Precision U-Series Dating of Corals from Western-Australia and Implications for the Timing and Duration of the Last Interglacial. *Earth Planet Sc Lett* **135**, 115-130.

67.Stringer, C. and C. Gamble. 1993. *In Search of the Neanderthals: Solving the Puzzle of Human Origins.* New York: Thames and Hudson.

68.Szabo, B. J., Ludwig, K. R., Muhs, D. R. & Simmons, K. R. 1994. Th-230 Ages of Corals and Duration of the Last Interglacial Sea-Level High Stand on Oahu, Hawaii. *Science* **266**, 93-96.

69.Thomas, A. L. et al. 2009. Penultimate Deglacial Sea-Level Timing from Uranium/Thorium Dating of Tahitian Corals. *Science* **324**, 1186-1189.

70.Thompson, W. G. & Goldstein, S. L. 2005. Open-system coral ages reveal persistent suborbital sea-level cycles. *Science* **308**, 401-404.

71.Thompson, W.G., and S.L. Goldstein. 2006. A radiometric calibration of the SPECMAP timescale. *Critical Quaternary Stratigraphy* **25**, 3207-3215.

72.Todhunter, I. 1886. *Spherical Trigonometry* (5th ed.). MacMillan.

73.Toscano, M. A. & Lundberg, J. 1999. Submerged Late Pleistocene reefs on the tectonically-stable SE Florida margin: high-precision geochronology, stratigraphy, resolution of Substage 5a sea-level elevation, and orbital forcing. *Quaternary Sci Rev* **18**, 753-767.

74.Turney, C.S.M., and Brown, H., 2007. Catastrophic early Holocene sea level rise, human migration and the Neolithic transition in Europe. *Qua. Sci. Rev.* **26**, 2036-2041.

75.Veeh, H.H., and Chappell, J. 1970. Astronomical Theory of Climatic Change: Support from New Guinea. *Science*, Vol.**167**, 862-865.

76.Waelbroeck, C, L. Labeyriea, E. Michel, J.C. Duplessy, J.F. McManus, K. Lambeck, E. Balbon, M. Labracherie. 2002. Sea-level and deep water temperature changes derived from benthic foraminifera isotopic records. *Quaternary Science Reviews* **21**, 295-305.

77.Wessel, Pill, Smith. Walter H.F. 1996. A global self-consistent, hierarchical, high-resolution shoreline database. *Journal of Geophysical Research* **101** No. B4, 8741-8743

78.Wilcoxon, F. and Wilcox, R.A., 1964. Some rapid approximate statistical procedures. Lederle Laboratories.

79.Wright, J.D., Sheridan, R.E., Miller, K.G., Uptegrove, J., Cramer, B.S., and Browning, J.V.2008. Late Pleistocene Sea level on the New Jersey Margin: Implications to eustasy and deep-sea temperature. *Global and Planetary Change* **66**, 93-99.

80.Yokoyama, Y., Esat, T. M. & Lambeck, K. 2001. Coupled climate and sea-level changes deduced from Huon Peninsula coral terraces of the last ice age. *Earth Planet Sc Lett* **193**, 579-587.

81.Yokoyama, Y., Lambeck, K., De Deckker, P.P.J., Fifielf, L.K., 2000. Timing of the last glacial maximum from observed sea-level minima. *Nature* **406**, 713-716.

82.Yue, S., Pilon, P., Phinney, B. & Cavadias, G. 2002b. The influence of autocorrelation on the ability to detect trend in hydrological series. *Hydrol. Processes* **16**, 1807–1829

83.Zhu, Z. R. et al. 1993. High-Precision U-Series Dating of Last Interglacial Events by Mass-Spectrometry - Houtman-Abrolhos Islands, Western-Australia. *Earth Planet Sc Lett* **118**, 281-293.

8. Appendix

Global sea level change.avi

https://www.youtube.com/watch?v=hmYZ3SlXjTk&feature=youtu.be